Osaka University Knowledge Archive

Title	Evolution of Slow-Binding Inhibitors Targeting Histone Deacetylase Isoforms
Author(s)	Mukherjee, Anirban; Zamani, Farzad; Suzuki, Takayoshi
Citation	Journal of Medicinal Chemistry. 2023, 66(17), p. 11672-11700
Version Type	AM
URL	https://hdl.handle.net/11094/93985
rights	This document is the Accepted Manuscript version of a Published Work that appeared in final form inJournal of Medicinal Chemistry, © American Chemical Society after peer review and technical editing by the publisher. To access the final edited and published work see https://doi.org/10.1021/acs.jmedchem.3c01160.
Note	

Osaka University Knowledge Archive : OUKA

https://ir.library.osaka-u.ac.jp/

Osaka University

Evolution of Slow-Binding Inhibitors Targeting Histone Deacetylase Isoforms

Anirban Mukherjee[‡], Farzad Zamani[‡], and Takayoshi Suzuki*

SANKEN, Osaka University, Mihogaoka, Ibaraki-shi, Osaka 567-0047, Japan.

SIGNIFICANCE

- Drugs with longer residence times exhibit enhanced and sustained *in vivo* activity within animal models, potentially serving as an indicator of the drug's effectiveness.

- This perspective focuses on the recent development of slow-binding inhibitors designed to target specific HDAC isoforms through a critical understanding of the existing approaches.

- It accentuates limitations and explores potential future directions within the field of HDAC inhibitor development, fostering a deeper comprehension of multifaceted issues through a scientifically driven narrative.

ABSTRACT

Because the overexpression of histone deacetylase enzymes (HDACs) has been linked to numerous diseases, including various cancers and neurodegenerative disorders, HDAC inhibitors have emerged as promising therapeutic agents. However, most HDAC inhibitors lack both subclass and isoform selectivity, which leads to potential toxicity. Unlike classical hydroxamate HDAC inhibitors, slow-binding HDAC inhibitors form tight and prolonged bonds with HDAC enzymes. This distinct mechanism of action improves both selectivity and toxicity profiles, which makes slow-binding HDAC inhibitors a promising class of therapeutic agents for various diseases. Therefore, the development of slow-binding HDAC inhibitors that can effectively target a wide range of HDAC isoforms is crucial. This perspective provides valuable insights into the potential and progress of slow-binding HDAC inhibitors as promising drug candidates for treating various diseases.

INTRODUCTION

Although small drug molecules still hold a prominent position in drug discovery, new modalities have been added to drug discovery technologies. In the early phase of drug development, medicinal chemists usually optimize the structure of lead compounds based on their thermodynamic signatures (IC_{50} and K_d). During the optimization, entropic and enthalpic contributions to the binding are both determined. Although the optimization of favorable binding enthalpies is extremely difficult, highly system-specific effects, such as hydrogen bonding and van der Waals interactions, provide favorable enthalpic contributions and are considered as primary driving forces for binding.[1] These assessments are often performed in cell-free assays by evaluating ligand binding under equilibrium conditions in a closed system. Accordingly, the target is exposed to a constant ligand concentration throughout the experiment, which poorly simulates the ideal environment of an open system corresponding to that of the human body.[2-5] In open systems, ligand/protein concentrations vary over time, and it is difficult to represent and anticipate the amount of formed ligand–protein complexes and the physiological response. To overcome these limitations, it is also important to evaluate inhibitor–protein bindings based on kinetic parameters of the binding interaction and include them in the drug design process.[6] One promising approach for optimizing kinetic parameters of the ligand binding is the application of the drug–target residence time model.[3] The concept of the drug–target residence time (t_R) has been advanced as a useful *in vitro* parameter that can complement traditional potency measurements, such as K_d, IC_{50}, and EC_{50}, for predicting a drug's *in vivo* effectiveness. Unlike these traditional measures, t_R is a kinetic parameter that is not influenced by variations in enzyme and drug concentrations and more closely resembles the dynamics of *in vivo* systems, wherein equilibrium is never truly achieved because drugs are constantly associating with and dissociating from their targets. In this concept, t_R refers to the lifetime of a drug–target complex and describes how long a drug is bound to its intended target,

3

which can be determined based on the reciprocal of the dissociation rate constant, k_{off} (t_R = $1/k_{off}$).[3-6] The residence time is associated with the duration of the pharmacological effect of a drug in an *in vivo* setting;[3,4] that is, the longer the target biomolecule is bound to a ligand, the longer the drug remains efficacious in an open system. In theory, the lifetime of a drug–target complex is extended by a slow dissociation, which highly depends on k_{off}.[5] Accordingly, recent studies have emphasized the importance of t_R for estimating a drug's *in vivo* efficacy. However, the prediction of the precise effect of t_R on a drug's *in vivo* efficacy can sometimes be challenging, particularly when the dissociation rate constant (k_{off}) is so low that it cannot be accurately determined. For example, researchers have found that t_R would likely negligibly impact a drug's *in vivo* efficacy if the drug's elimination half-life is longer than its t_R[7] because the *in vivo* pharmacological activity is primarily controlled by the drug's concentration when the concentration exceeds the drug's binding affinity. Notably, however, *in vitro* measurements of t_R using diluted enzymes may not fully explain possible rebinding mechanisms, which could further prolong drug–target binding *in vivo*.[8] Therefore, the drug's concentration primarily determines the drug's activity *in vivo* and is mostly influenced by both the drug's residence time and elimination half-life ($T_{1/2}$).

A drug's target selectivity is usually measured with respect to thermodynamic binding parameters, such as IC_{50} and K_d. However, this static definition of selectivity does not include the residence time on the target compared with those on off-target biomolecules. Therefore, the drug selectivity should also be considered as a time-dependent parameter.[2-5] Additionally, t_R impacts the selectivity of a drug's interaction with pharmacological proteins.[9,10] If a drug has a long residence time on its target, the drug's pharmacokinetic lifetime is exceeded during the systematic circulation, which can lead to a high selectivity for the intended target.[2-5] Recent studies have suggested that prolonged *in vivo* drug–target binding can protect drugs against being metabolized by minimizing both the drugs' binding to other proteins, including metabolic

enzymes, and excretion. This could explain why certain compounds may exhibit an unexpectedly long elimination half-life.[8] This increased selectivity, also known as the "kinetic selectivity", provides a substantial safety advantage to medications with long residence times in open systems. Therefore, ideal potent and selective drugs for clinical applications exhibit both thermodynamic (IC_{50} and K_d) and kinetic selectivity (residence time) toward its intended target.

1. Slow-binding enzyme inhibitors

Enzymes are prime drug-discovery targets because the modulation of the enzymatic activity can have rapid and distinct biological effects. Approximately 50% of all medications work by inhibiting enzyme functions through interactions with enzyme active sites.[11] Reversible enzyme inhibition is the most common action mode of enzyme inhibitors and often rapidly (high on/off rates) equilibrates the enzyme (E), inhibitor (I), and enzyme–inhibitor (E:I) complex within microseconds. However, recent enzymatic studies have shown that enzymes do not immediately respond to inhibitors but rather slowly inhibit them. These inhibitors are called "slow-binding inhibitors," which require lag times of seconds to days to reach steady-state inhibition ranges. This concept is related to sustained drug–target complexes exhibiting extended residence times on targets. In other words, for slow-binding inhibitors exhibiting a low drug–target dissociation rate, the drug occupancy time on the target remains prolonged, even if the effective inhibitor concentration quickly decreases in the systematic circulation. Therefore, compared with fast-binding inhibitors, slow-binding and -dissociating inhibitors should offer several advantages, such as slower pharmacokinetics and prolonged pharmacological effects *in vivo*, lower dosages, and fewer associated toxicities and side effects.[4,12]

In slow-binding enzymatic inhibition, the inhibition degree at a fixed inhibitor dosage changes over time, and the free and enzyme-bound forms of the inhibitor slowly equilibrate. Reaction mechanisms A and B have mainly been proposed to explain slow-binding enzymatic inhibition (Scheme 1).[13,14] Mechanism A suggests that the E:I complex directly forms in a single slow step without generating any kinetically detectable intermediates, where k_1 (k_{on}) and k_{-1} (k_{off}) are quite low compared with the rate constants ([S] K_m^{-1} and k_{cat}) for converting a substrate (S) to a product (P). This indicates that the Michaelis–Menten (E:S) complex instantly forms, while the E:I complex slowly forms and dissociates, resulting in a slow enzymatic inhibition. In mechanism B, a moderate-affinity E:I complex initially forms rapidly and then slowly isomerizes to another stable high-affinity E:I* complex, and k_1 (k_{on}) and k_{-1} (k_{off}) are assumed to be higher than k_2 and k_{-2}, respectively. In mechanism B, because the inhibitor affinity is not achieved until the E:I* complex forms, the slow-binding inhibitor affinity should be measured based on K_i, k_2, and k_{-2}.
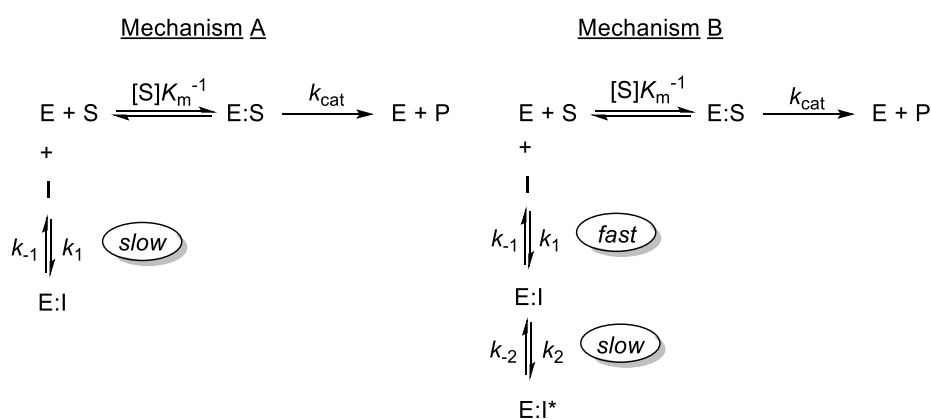
Scheme 1. Mechanistic pathways of slow-binding enzymatic inhibition.

Mechanisms A and B can be distinguished by analyzing reaction time courses with respect to initial substrate and inhibitor concentrations ([S] and [I], respectively).[15] When a conventional fast-binding inhibitor is used and the substrate is not markedly depleted, the

kinetic curve for the reaction is linear. When a slow-binding inhibitor is used, on the other hand, the product forms in a manner similar to that during the reaction's transient phase; that is, the reaction initially proceeds rapidly and then equilibrates to a slow steady state, wherein the kinetic curve for the reaction becomes asymptotic.[16]

Therefore, slow-binding inhibitors are compounds that inhibit their target enzymes in a time-dependent manner by considering their residence time on the appropriate target. Because of this unique feature, the target residence time of slow-binding HDAC inhibitors on different classes/isoforms of HDAC, is also different, which helps to induce selectivity toward each class/isoform. Such precision offers potential benefits in personalized therapies and optimized drug development, promising more effective treatments with reduced side effects.

2. Histone deacetylases (HDACs) and HDAC inhibitors

Histone deacetylases (HDACs) are a class of epigenetic regulators that play important roles in remodeling the chromatin structure and regulating gene expression by catalyzing the lysine deacetylation of histones.[16,17] Additionally, HDACs play various biological functions including metabolism, angiogenesis, DNA damage response, apoptosis, immunity, and protein degradation. Eighteen mammalian HDACs have been identified and classified into four groups based on their homology to yeast deacetylases. These groups include Rpd3/Hda1, which is a family of Zn^{2+}-dependent enzymes comprising classes I (HDAC1, HDAC2, HDAC3, and HDAC8), IIa (HDAC4, HDAC5, HDAC7, and HDAC9), IIb (HDAC6 and HDAC10), and IV (HDAC11). Furthermore, class III HDACs, also known as sirtuins (SIRT1-7), are nicotinamide-dependent enzymes that are related to yeast sirtuins.[16,17] The HDAC length ranges from 347 to 1215 amino acids for the shortest and longest HDACs (11 and 6), respectively.[18] The HDAC active site comprises an 11 Å deep pocket containing a zinc ion.[19] Zn^{2+}-dependent HDACs use this zinc ion to facilitate the lysine deacetylation of histones,

whereby the lysine (or inhibitor) passes through the tubular access to reach the zinc ion.[19] When the active site is activated by a metal ion, a water molecule attacks the *N*-acetyl group, resulting in the formation of nitrogen-free lysine and a metal-ion-stabilized acetate byproduct. Within the active site, although Zn^{2+}-dependent HDACs exhibit a similar zinc-ion environment, some residues are different. This environment comprises two histidine–aspartic acid pairs and a tyrosine residue, and the zinc ion firmly couples to two aspartic acids and one histidine residue.[20]

Given the diverse biological functions of HDACs, it is not surprising that the aberrant expression of HDACs is associated with many cancers, inflammatory diseases, and aging-related neurological disorders, such as Alzheimer's and Parkinson's diseases.[21-24] Consequently, HDAC inhibitors have attracted considerable attention as promising therapeutic agents for such diseases and were the first class of epigenetic drugs approved for treating cancer. HDAC inhibitors share a well-accepted pharmacophore model (Figure 1) comprising a zinc-binding group (ZBG) attached to a linker that mimics the lysine side chain and occupies the tubular access through which the lysine substrate reaches the catalytic domain. The linker is terminated by a functional capping group that interacts with the external surface of the channel entrance.[18,20,25,26] Over the past few decades, numerous HDAC inhibitors have been identified and can be categorized as hydroxamic acid derivatives, benzamides, carboxylic acid derivatives, and cyclic peptides. Some of these inhibitors, including vorinostat, belinostat, and romidepsin, have recently been approved by the U.S. Food and Drug Administration (FDA) for treating various T-cell lymphomas or multiple myeloma.[27] However, despite substantial developments toward HDAC inhibitors in drug discovery, their clinical applications are still limited owing to intense adverse effects and toxicities caused by the poor isoform selectivity of HDACs. Ideally, selective HDAC inhibitors would serve as valuable chemical tools to understand the distinct functions of each HDAC. Specifically, such selective inhibitors would help reveal the

molecular mechanisms linking HDAC activity to the development of human diseases. Moreover, it is plausible that a selective HDAC inhibitor could offer more effective chemotherapy compared to non-selective HDAC inhibitors. Table 1 presents a summary of recent discoveries regarding selective HDAC inhibitors and their biological mechanisms/effects in cells.[28-39] Although many HDACs are highly conserved and share sequential similarity among HDAC classes, such as I and IIa, HDACs play various roles for regulating epigenetics. For example, previous studies have indicated that HDAC3 is a key class I HDAC for modulating inflammatory gene expression by regulating the nuclear factor κB (NF-κB) pathway.[28] Therefore, the selective targeting of HDAC3 in the NF-κB pathway is a promising strategy for treating inflammatory diseases (Table 1). In principle, the application of an unselective HDAC inhibitor for targeting multiple HDAC isoforms may result in mechanism-based toxicities, such as thrombocytopenia, and diminish the therapeutic efficacy.[40] For example, FDA-approved vorinostat is a rather unselective potent HDAC inhibitor that inhibits most Zn^{2+}-dependent HDAC isoforms, including HDAC1–3 and HDAC8, HDAC6 and HDAC7, and HDAC11 (Classes I, II, and IV, respectively).[41] Multiple clinical trials evaluated vorinostat as a single therapy in patients have shown that this medication displays several high-grade toxicities, including dehydration, thrombocytopenia, and cardiac abnormalities.[42] Owing to the isoform selectivity of HDAC inhibitors, numerous studies have recently been conducted for developing selective HDAC inhibitors for specific isoforms.[43,44] Although many efforts have been made to identify isoform-selective HDAC inhibitors by modulating the ZBG, linker, and cap group,[18-27] additional studies are required. Most previous studies have focused on thermodynamic binding parameters (IC_{50} and K_d). These activity/selectivity analyses only statically define activity/selectivity and do not include residence times on target and off-target biomolecules. Because these measurements poorly mimic the ideal environment of an open system similar to that of the human body, the

optimization of inhibitor binding kinetics toward each isoform, also known as "kinetic selectivity", is a highly recommended prerequisite for developing isoform-selective HDAC inhibitors for clinical applications.
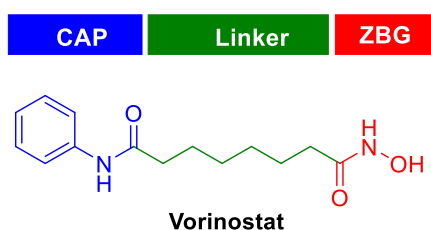

Figure 1. Structure of histone deacetylase (HDAC) inhibitors. Vorinostat is the first HDAC inhibitor approved by FDA for treating cancer.

Table 1. Summary of biological effects/mechanisms of class-selective Zn-dependent HDAC inhibitors.

HDAC inhibitor	Biological effects	Mechanism of action
Class I[21,28-32]	– Anti-inflammatory activity	– Inhibiting NF-kB activation pathway. – Inhibiting pro-inflammatory gene expression.
	– Anti-cancer activity	– Upregulating tumor suppressor genes such as p21 and p27 – Downregulating the survival protein Bcl-2. – Upregulating p53, pVHL, thrombospondin 1, and anti-angiogenic activin A transcription. – Downregulating HIF-1α, VEGF, and FGF. – Increasing overall fatty acylation levels. – Promoting cell cycle arrest at G2/M phase. – Interfering with the homologous recombination repair pathway of DNA. – Inhibiting angiogenesis.
	– Anti-obesity activity	– Inhibiting adiponectin gene expression to improve glucose tolerance.
	– Activity in neurological disorders	– Enhancing FXN mRNA and frataxin protein levels in FRDA neurons.
Class IIa[33,34]	– Anti-cancer activity	– Inhibiting ERK1/2 signaling pathway. – Inducing recruitment and differentiation of highly phagocytic and stimulatory macrophages within tumors. – Inhibiting abolishes NO-induced formation of macromolecular complexes.
	– Anti-inflammatory activity	– Reducing pulmonary arterial hypertension and cerebral ischemia/reperfusion injury. – Suppression of myocyte hypertrophy.
	– Immunostimulatory activity	– Decreasing downstream hypoxia-inducible factor (HIF)-VEGF signaling.
Class IIb[29,35,36]	– Anti-cancer activity	– Inducing mtp53 degradation. – Reducing MDSCs proportion. – Inhibiting abnormal DNA damage and hyper cytokine and growth factor responses.

|		
	– Improving cognitive function	– Enhancing the synaptic activities of PC_{12} and SH-SY$_5$Y neuronal cells.
Class IV[37-39]	– Anti-cancer activity	– Induction of the proapoptotic genes such as Bmf and Bim.
	– Antiviral activity	– Regulating type I interferon signaling.
	– Anti-obesity activity	– Increasing fatty acylation level of SHMT2. – Induction of uncoupling protein 1 (UCP1) expression and activity. – Activating the adiponectin-AdipoR-AMPK pathway in the liver.

3. Slow-binding HDAC inhibitors

The "residence time" concept is important for the early-phase drug discovery of HDAC inhibitors. A slowly dissociating isoform-selective HDAC inhibitor should exhibit a longer residence time on the target HDAC isoform (which may require lower dosages of the HDAC inhibitor), a prolonged effect on histone deacetylation, and fewer toxicities in patients.[45] Studies recently conducted in both cell-based *in vitro* and *in vivo* settings have supported this hypothesis for kinetically isoform-selective HDAC inhibitors.[46-50] To target a specific HDAC isoform, the binding kinetics of an HDAC inhibitor can be tuned based on the structure–activity relationship (SAR) analysis of the substituent size, regiochemistry, and ligand hydrophobicity. Although several reviews have reported the synthesis methodologies, binding thermodynamics, and clinical drug development of HDAC inhibitors,[18-24,26,27] to the best of our knowledge, the importance of the optimization of binding kinetic parameters for developing potent *in vivo* isoform-selective HDAC inhibitors has rarely been mentioned. Therefore, this perspective focuses on the development of kinetically isoform-selective slow-binding HDAC inhibitors, especially their binding kinetics and action mechanisms, to highlight the impact of kinetic parameters for designing HDAC inhibitors for clinical applications. In the following sections, the activities and kinetic selectivity of various classes of slow-binding HDAC inhibitors are discussed. The connection among the kinetic binding parameters, mechanistic information, and

chemical structures of compounds is a vital tool for optimizing the drug design for clinical applications.

3.1. Slow-binding class I HDAC inhibitors

In 2008, Gottesfeld *et al.* initially reported the benzamide-based slow-binding inhibition of class I HDACs.[49] Benzamide HDAC inhibitors were initially considered as weak inhibitors owing to their high IC_{50} for HDACs. However, cell-based and mouse models revealed that benzamide HDAC inhibitors have unique biological functions, outstanding subtoxic efficacies, and effective deacetylase IC_{50} values for Friedreich's ataxia (FRDA) and Huntington's disease.[51,52] This confusion motivated the authors to investigate the kinetic properties of a pimelic diphenylamine inhibitor **1** with recombinant human HDACs. The authors found that the benzamide HDAC inhibitor **1** is a slow-binding inhibitor of HDAC1, HDAC2, and HDAC3 and IC_{50} values varied depending on the preincubation period. For example, **1** showed IC_{50} values of 460 and 5800 nM for HDAC1 and HDAC3, respectively, without any preincubation. However, after preincubation of 15 min, the IC_{50} value for HDAC1 equilibrated at 138 nM. For HDAC3, several more hours of preincubation were required for **1** to reach a steady-state value. After preincubation of 3 h, IC_{50} dropped to 380 nM, which is an approximately 15-fold reduction compared with the IC_{50} value measured without any preincubation. Therefore, IC_{50} values will not likely produce consistent results unless the equilibration of the inhibitor and enzyme is ensured. Because kinetic parameters (K_i, k_{on}, and k_{off}) are intrinsic properties of enzyme–inhibitor pairs, they are constants used for accurately estimating a compound's inhibition for its target enzyme. Benzamide **1** exhibited a high kinetic selectivity for HDAC3, for which K_i values were 148, 102, and 14 nM for HDAC1, HDAC2, and HDAC3, respectively, which could not be captured by IC_{50} measurements. Additionally, kinetic measurements indicated that **1** inhibited both HDAC1 and HDAC2 through mechanism A (Scheme 1) in a

competitive slow-binding manner, while forming a stable complex with HDAC3 *via* a slow step (mechanism B in Scheme 1), for which $t_R \approx 12$ h. The formation of a stable enzyme–inhibitor complex between inhibitor **1** and HDAC3 extended the drug–target residence time and prolonged the histone acetylation, which upregulated the frataxin gene. Furthermore, a 100-fold dilution of the enzyme/inhibitor mixture exhibited a negligibly decreased inhibition within 1 h. In contrast, the inhibitory effect of vorinostat was immediately lost within minutes after the dilution, indicating that this compound rapidly dissociated from HDACs. Furthermore, MTS cell proliferation assays revealed that cells treated with compound **1** lost a trace of acetylated histone H3 even after the removal of the inhibitor for 7 h. The acetylation of histone H3, on the other hand, was lost in vorinostat-treated cells within the first hour after the inhibitor was removed, which suggests that the investigation of relative inhibitory activities based on IC_{50} values may not be an accurate method for screening potentially useful and important HDAC inhibitors for clinical applications.
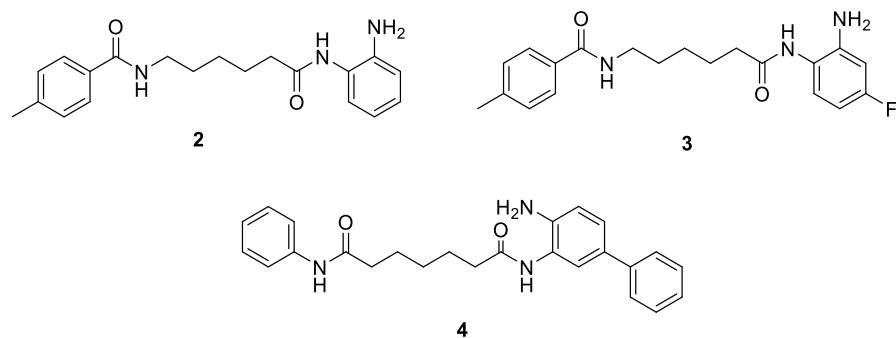

1
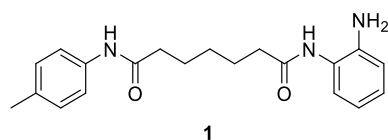
	HDAC1		HDAC3	
	1	**Vorinostat**	**1**	**Vorinostat**
K_i	148 nM	5.4 nM	14 nM	7.8 nM
k_1	4.9×10^4 M^{-1} min^{-1}	-	-	-
k_{-1}	0.0072 min^{-1}	-	-	-
k_2	-	-	0.021 min^{-1}	-
k_{-2}	-	-	0.00143 min^{-1}	-
$T_{1/2}$	~ 1.5 h	-	~ 8 h	-
t_R	-	-	~ 12 h	-

Figure 2. Chemical structure and kinetic parameters of class I HDAC inhibitor **1**.

FRDA is a rare genetic disease caused by the hyperextension of a GAA–TTC triplet in the FXN gene's first intron, which encodes the essential mitochondrial protein frataxin.[53] Post-

translational modifications of histones near expanded repeating units are consistent with the formation of heterochromatin and subsequent FXN gene silencing. Although HDAC inhibitors can enhance FXN mRNA and frataxin protein levels in FRDA neurons, recent studies have revealed that only compounds that selectively target class I HDAC1 and HDAC3 can increase the FXN gene expression in iPSC-derived FRDA neurons.[54] Benzamide-based inhibitors can upregulate the frataxin gene expression by inhibiting HDAC3, which make these compounds promising therapeutic drugs for treating such diseases. Pandolfo *et al.* developed a strategy for improving the pharmacological profile of benzamide-based inhibitors.[55] Benzamide HDAC inhibitors **2** and **3** (Figure 3) were synthesized and tested in a KIKI mouse model and peripheral blood mononuclear cells (PMBCs) collected from FRDA patients. Although the overall potency and selectivity degree against HDAC3 were much higher for compound **2** than compound **3** (Figure 3), **2** was effective for PMBCs, while **3** displayed a high efficacy in the KIKI mouse model. Compound **2** showed an approximately 4- to 9-fold frataxin upregulation and a good dose–response correlation for PMBCs. Compound **3**, on the other hand, was efficacious at a 3-fold lower dosage in the KIKI mouse model. Moreover, for compound **3**, IC_{50} decreased from 16.8 to 560 nM over 3 h for HDAC3/NcoR2. In contrast, compound **3** did not show any time-dependent behavior for inhibiting HDAC1. For compound **2**, IC_{50} dropped from 230 to 60 nM within 1 h and from 1 to 50 nM over 3 h for HDAC1 and HDAC3/NcoR2, respectively, indicating that the inhibition of both HDAC1 and HDAC3/NcoR2 showed time-dependent behaviors. Furthermore, K_i values revealed that compounds **2** and **3** showed 6- and 3-fold selectivities for HDAC3 and 1, respectively. Gottesfeld *et al.* previously reported the benzamide-based slow-binding inhibition of HDAC3.[49] Their results and the determined K_i values suggest that compound **2** is a slow-binding inhibitor for both HDAC1 and HDAC3/NcoR2 and that compound **3** is a selective slow-binding inhibitor for HDAC3/NcoR2. However, the authors did not investigate the reason for this slow-binding inhibition behavior

(long residence time). Furthermore, Gottesfeld *et al.* reported that HDAC inhibitors selectively targeting either HDAC1 or HDAC3 did not show similar increased FXN mRNA levels.[56] The authors investigated the kinetic properties of HDAC inhibitors **2–4** to understand the action mechanism. Compound **3** displayed approximately 3-fold selectivity for HDAC3 compared with HDAC1, for which K_i values were 196 and 630 nM, respectively, and functioned as both fast-binding HDAC1 and slow-binding HDAC3 inhibitors ($t_R = 1.2$ h, Mechanism B in Scheme 1). For HDAC1, the competitive inhibition mechanism of compound **2** is similar to that of vorinostat and other hydroxamate HDAC inhibitors, which fail to activate the FXN gene expression.[51] Compound **4** exhibited an approximately 350-fold selectivity for HDAC1 compared with HDAC3, for which K_i values were 7.0 and 2500 nM, respectively. The kinetic data showed that compound **4** inhibited HDAC 1 and HDAC3 through slow-binding mechanisms B ($t_R = 9.8$ h) and A (Scheme 1), respectively, where a stable ligand/enzyme complex did not form. Additionally, after FRDA iPSC-derived neurons were incubated with compound **4**, the quantitative reverse transcription–polymerase chain reaction (qRT–PCR) analysis revealed that compound **4** slightly affected FXN mRNA levels. Compound **2** exhibited an approximately 6-fold selectivity for HDAC3 compared with HDAC1, for which K_i values were 5 and 32 nM, respectively, which indicated that compound **2** inhibited both HDAC 3 and HDAC1 through a slow-binding mechanism (B). Additionally, compound **2** displayed high potency for inducing the FXN gene expression in FRDA iPSC-derived neurons. These observations strongly suggest that the simultaneous inhibition of HDAC 1 and HDAC3 *via* a slow-binding inhibition mechanism, B (stable target engagement and long residence time), is required for reactivating the FXN gene in neurons.

Figure 3. Chemical structures and kinetic parameters of class I HDAC inhibitors **2–4**.

	HDAC1				HDAC3					
	k_2 (min^{-1})	k_{-2} (min^{-1})	K_i (nM)	t_R (h)	k_2 (min^{-1})	k_{-2} (min^{-1})	k_1 (min^{-1}M^{-1})	k_{-1} (min^{-1})	K_i (nM)	t_R (h)
2	0.121	0.0036	32	4.6	0.0762	0.0025	-	-	5	6.7
3	-	-	630	-	0.124	0.0136	-	-	196	1.2
4	0.1675	0.0017	7	9.8	-	-	600	0.0015	2500	-

The dysfunction of pancreatic β-cells is a common cause of diabetes, and HDAC inhibitors have been found to play a pivotal role in the preservation of β-cells, suggesting potential therapeutic applications for the treatment and the implication of HDACs in such diseases. To elucidate the underlying mechanism and involvement of specific HDAC isoforms, Wagner *et al.* designed anilide tacedinalines **5** and **6** as selective and potent inhibitors of class I HDACs (Figure 4).[48] The C_5-substituted anilide **5** showed more than 110-fold-higher selectivity for HDAC 1 and HDAC2 (IC$_{50}$ = 2 and 19 nM, respectively) compared with HDAC3 (IC$_{50}$ = 2080 nM), while a fluoro-substitution at the C_4 position of **6** led to a >17-fold-higher selectivity for HDAC3 (IC$_{50}$ = 64 nM) compared with HDAC 1 and HDAC2 (IC$_{50}$ = 1080 and 1150 nM, respectively). The binding kinetic analysis revealed that compound **6** selectively bound to HDAC3 (K_i = 0.029 μM) through a fast-on/slow-off mechanism (k_{on} = 0.3 min^{-1}μM^{-1}; k_{off} = 0.0088 min^{-1}) with >170-fold selectivity, suggesting that the longer residence time (t_R = 1.9 h) of compound **6** on HDAC3 compared with that of compound **6** on HDAC1 and HDAC2 is the key for the selective inhibitory effect of compound **6**. Computational investigations revealed that interactions between the leucine residue and either HDAC3 or HDAC2 were

different in the binding pocket. In this case, the specificity of compound **6** was attributed to the slightly larger internal cavity of the HDAC3 binding domain, which stabilized the compound through a π-interaction with one of the methyl groups of the Leu133 and Tyr107 residues. Therefore, compound **6** exactly fit the binding pocket without affecting the Leu133 residue, and the most favorable geometry was achieved using the fluoro-substituted anilide, which is a considerably smaller molecule and has a considerably lower electron density than compound **5**. These results emphasize the crucial role of the leucine residue for determining the selectivity. Compound **6** protected pancreatic β-cells from inflammatory cytokines, reduced hyperglycemia, increased insulin secretion, and suppressed cellular apoptosis, all while exhibiting a useful biological activity through the kinetically selective inhibition of HDAC3 and avoiding mechanism-based toxicities.
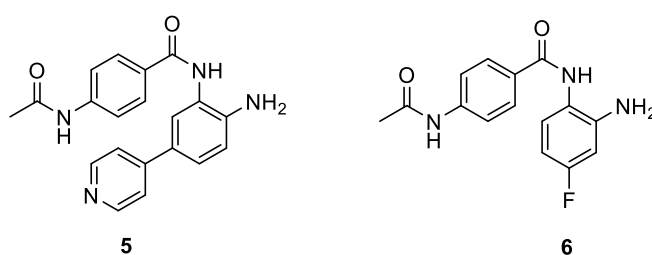
	5			6		
	HDAC1	HDAC2	HDAC3	HDAC1	HDAC2	HDAC3
k_{on} (min^{-1}μM^{-1})	0.624	0.028	0.0011	0.020	0.0082	0.3
k_{off} (min^{-1})	0.0016	0.0004	0.0016	0.27	0.052	0.0088
$T_{1/2}$ (min)	430	~1800	690	2.5	13	79
K_i (μM)	0.003	0.014	14.0	5.1	6.3	0.029
t_R (h)	10.4	41.7	10.4	~ 0.1	0.3	1.9

Figure 4. Chemical structures and kinetic parameters of class I HDAC inhibitors **5** and **6**.

A lengthened QT interval and heartbeat irregularities can be caused by the inhibition of the human ether-a-go-go-related gene (hERG) channel. Studies have shown that because HDAC inhibitors may inhibit hERG and potently inhibit deacetylase,[57] selective HDAC

inhibitors that do not bind to hERG should be urgently developed. To solve this problem, Methot *et al.* designed and synthesized a biaryl nicotinamide (**7**) containing a spirocyclic carbamate moiety (Figure 5).[58] Although compound **7** exhibited a potent inhibitory activity against HDAC1 and HDAC2 (IC_{50} = 6 and 45 nM, respectively), it was almost inactive in the hERG binding assay (hERG K_i >30 µM). Interestingly, compound **7** required approximately 4 h to completely inhibit both HDAC1 and HDAC2 activities. Kinetic experiments also revealed that the inhibitor dissociated from HDAC1 relatively slowly, for which the half-life was over 100 min. The authors suggested that this slow-binding behavior was due to the necessary protein movement to accommodate the biaryl in HDAC1 and HDAC2 internal cavities. Furthermore, HCT116 colon carcinoma cells treated with compound **7** exhibited the time-dependent hyperacetylation of several histone residues, including lysine 5 of histone H2B (H2BK5), starting 4–8 h after the treatment and peaking at 96 h. This behavior was consistent with the slow-binding kinetics of compound **7**. A mouse HCT116 xenograft tumor model was then used to validate the *in vitro* findings. Mice were randomly divided into groups of 12 and given different oral doses of compound **7**. Then, their tumors were removed to isolate histones. After 24 h, the histone acetylation increased by approximately six times, remained approximately four times higher after 72 h, and persisted even after the drug was eliminated from the plasma. These findings revealed the slow off-rate binding kinetics of compound **7** through a prolonged target inhibition.
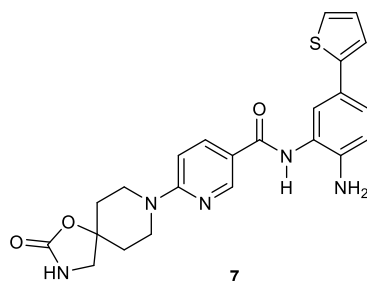

Figure 5. Chemical structure of class I HDAC inhibitor **7**.

Kral *et al.* developed an HDAC1/2-selective inhibitor **8** (Figure 6) and investigated its kinetic behavior.[59] Compound **8** showed a slow-binding behavior toward HDAC1, as indicated by a considerably decreased IC_{50} value with prolonged preincubation periods (Figure 6) and a dissociation rate constant (k_{off}) of 0.0086 min^{-1} ($t_R \approx 2$ h). This slow-binding behavior was attributed to a slow change in the enzyme conformation after the formation of the enzyme–inhibitor complex, wherein compound **8** occupied a hydrophobic "foot pocket" adjacent to the catalytic Zn^{2+} ion. In cellular assays using HCT116 human colon carcinoma cells, compound **8** delayed the deacetylation of histone H2B5K and maintained its effect, even after the compound was removed and showed a persistence superior to that of vorinostat. In a xenograft mouse model, immunodeficient CD1 nude/nude female mice were infected with HCT116 colon carcinoma cells and treated with compound **8** (either 150 mg/kg per day or 500 mg/kg twice per week) for three weeks. The results showed that the administration of compound **8** twice per week was enough to attain a therapeutic effect similar to that of vorinostat, which had to be administered daily. Furthermore, compound **8** produced a prolonged histone acetylation effect for 72 h, even after it was eliminated from the plasma.
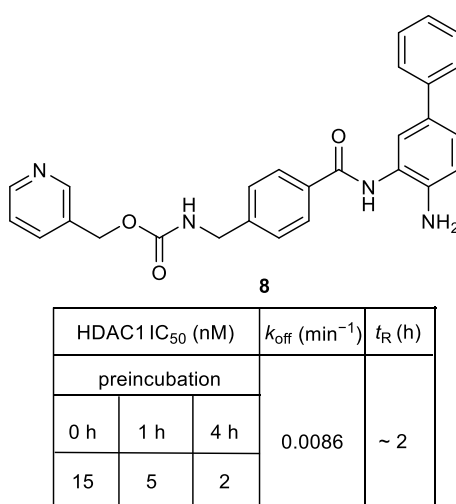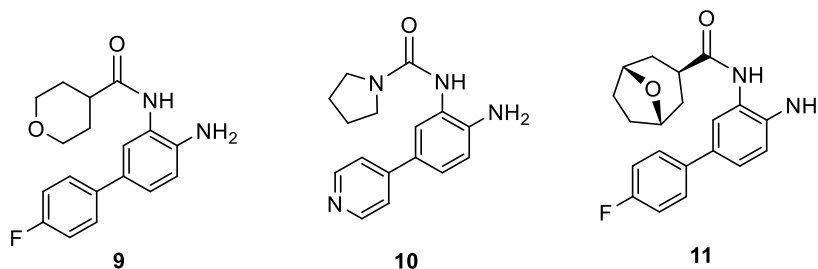

HDAC1 IC_{50} (nM)			k_{off} (min^{-1})	t_R (h)
preincubation				
0 h	1 h	4 h	0.0086	~ 2
15	5	2		

Figure 6. Chemical structure and kinetic parameters of class I HDAC inhibitor **8**.

Holson *et al.* modified inhibitor binding kinetics to selectively target HDAC2 for treating dementia by investigating a range of inhibitors containing *o*-aminoanilide as the ZBG.[46] The authors identified carbamate-based compound **9** and urea-based compound **10** (Figure 7a) as promising candidates that could effectively penetrate the blood–brain barrier. The kinetic analysis indicated that although compound **9** selectively inhibited HDAC2 more than HDAC1, the HDAC2 selectivity was only 7-fold according to k_{off} values (Figure 7a). Compound **10** displayed a 6-fold selectivity for inhibiting HDAC2. Additionally, the authors simulated target engagement profiles based on numerical integrations of a system of differential equations that described enzyme-state distributions.[46] Compounds **10** and **9** exhibited high and low degrees of HDAC2 target engagement of over 50 and up to 10%, respectively. The researchers enhanced the HDAC2 selectivity of compound **9** by manipulating the compound's binding kinetics in a 14 Å hydrophobic foot pocket at the zinc-binding site and found that amino acid residues in the pocket interacted with the *p*-fluorophenyl group of compound **9**. After testing several substituents, the authors concluded that the *p*-fluorophenyl group displayed the best binding properties. The crystal structure of the compound **9**–HDAC2 complex revealed a hydrogen-bonded water molecule that linked the pyran oxygen atom of compound **9** and His183 residue of HDAC2 (Figure 7b). Because of this finding, the researchers investigated different regioisomers of the hydrogen-bonded pyran ring and identified compound **11**, which exhibited an enhanced target engagement with HDAC2.[47] Compounds **11** and **9** showed 12- and 7-fold longer residence times on HDAC2 than on HDAC1, respectively (Figure 7a). In addition, compared with compound **9**, compound **11** showed higher on and off rates for HDAC1, which reduced the target engagement and shortened the residence time. The authors proposed that the selectivity of compound **11** for HDAC2 was attributed to van der Waals interactions between the compound and lipophilic channel's wall and rim, which displaced the Phe155 residue, and the adoption of an

energetically favorable chair conformation by the oxabicyclo-octane moiety, which enabled

the pyran ring's oxygen atom to interact with the bridging water molecule through a hydrogen

bond (Figure 7b).

(a)

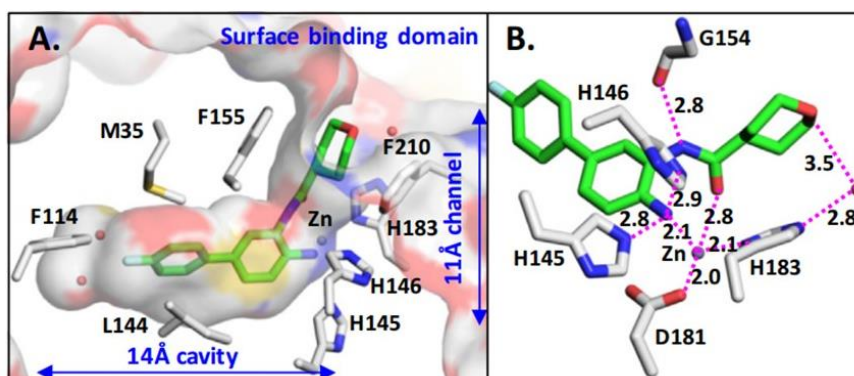| Compound	HDAC1			HDAC2		
	k_{on} (min^{-1} µM^{-1})	k_{off} (min^{-1})	t_R (min)	k_{on} (min^{-1} µM^{-1})	k_{off} (min^{-1})	t_R (min)
9	0.41	0.0345	29	0.014	0.0049	204
10	0.185	0.01065	94	0.00895	0.00182	550
11	1.23	0.217	5	0.036	0.019	53

(b)

Figure 7. (a) Chemical structures and kinetic parameters of class I HDAC inhibitors **9–11**; (b) X-ray crystallography structure of inhibitor **9** bound to HDAC2. (B) Interaction between the key amino acid residues and the complex of inhibitor **9** (green) binding to zinc ion (purple). Reproduced from reference 46. Reproduced with permission from [46]. Copyright [2015] [The Royal Society of Chemistry].

Various biochemical protocols, such as thermal shift and GFP-based stability assays

have been utilized to identify the ligand–target engagement based on ligand-induced protein

stabilization.[60,61] However, these methods frequently produce false negative results because

many ligand-bound protein targets do not display any measurable stabilization.[62] Additionally, some of these methods require high temperatures, which may not provide physiological conditions for ligand binding. These limitations make such techniques unsuitable for measuring the binding kinetics or ligand residence time. Bioluminescence resonance energy transfer (BRET) is an efficient method for monitoring molecular interactions within intact cells in real time and requires neither non-physiological temperatures nor cell lysis.[63] BRET is achieved through the reversible binding of a fluorescent tracer to an intracellular target. The ability of a ligand to compete with the tracer and, thus, influence BRET production reveals the ligand's binding characteristics; that is, the displacement of the tracer results in a loss of BRET. Robers *et al.* reported the first BRET application for directly measuring the target engagement and binding kinetics of the clinically approved HDAC inhibitor, romidepsin **12** (Figure 8) in HeLa cells under physiological conditions.[64] Natural-product HDAC inhibitors, such as romidepsin **12**, exhibit strong inhibition potency (in the nanomolar range) against class I HDACs by binding to both the catalytic site (Zn^{2+} atom) and surface on which the HDAC and substrate interact.[65] A previous study has shown that the pulsed treatment of cells with compound **12** resulted in a strong and prolonged inhibition of the class I HDAC activity.[66] However, whether the prolonged potency of **12** is due to the prolonged residence time on HDACs remains unknown. BRET analyses of **12** and vorinostat on HDAC1 revealed that **12** had a much longer residence time (120 min) than vorinostat, for which the residence time was approximately 20 min. These results indicate that the prolonged phenotypic effect of **12** is due to the stable binary complex between the inhibitor and HDAC1. The BRET assay can be used as an initial approach for investigating the residence time of various drugs on protein targets in cells by monitoring drugs' dissociation kinetics.
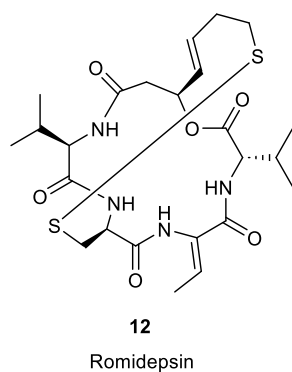
12

Romidepsin

Figure 8. Chemical structure of class I HDAC inhibitor, romidepsin **12**.

Cyclization plays a crucial role in the potency of macrocycle-based HDAC inhibitors. Although ZBG-free macrocycles can inhibit HDACs, their potencies are usually lower than those of their zinc-binding counterparts.[67,68] Because these inhibitors naturally contain a diverse range of ZBGs, the ascertainment of the importance of different macrocycles for the binding affinity and selectivity of HDAC isoforms is challenging. Therefore, the structural modification of these natural products can improve the understanding and benefit the design of high-binding-affinity HDAC inhibitors. Olsen *et al.* initially synthesized natural-product-derived macrocycles to determine their potency and selectivity for recombinant zinc-dependent HDAC isoforms (Figure 9). Then, the authors decorated a selection of scaffolds with various ZBGs or masked ZBGs and kinetically evaluated their modes of inhibition for various HDAC isoforms.[69] To assess the potency of non-zinc-binding compounds **13** and **14a–c**, their binding affinities were measured for recombinant HDAC1, HDAC2, and HDAC3 (Figure 9). Apicidin A **13** showed the highest binding affinities, for which $K_{i,1}$ was 0.40 and 0.60 μM for HDAC1 and HDAC3, respectively (Figure 9). Compared with its methyl- (**14b**), butyl- (**14c**), and hexyl- (**14d**) substituted derivatives, compound **14a**, which contains an *n*-propyl side chain, exhibited higher potencies for HDAC1, HDAC2, and HDAC3. Although all the selected non-zinc-binding compounds displayed acceptable potencies for HDACs, their potencies were considerably different. Although compounds **18** and **19** contained a strong zinc–hydroxamate

23

chelate and were anticipated to be more effective than their non-zinc-binding counterparts, **14a**–**14d** and **15**, respectively, they did not display remarkably improved potencies. These unforeseen results urged the authors to evaluate the inhibition mechanism through a further kinetic analysis. Analogs containing *n*-propyl (**14a**), ethyl ketone (**13**), and carboxylate (**16** and **17**) moieties showed a fast-on/fast-off binding mechanism, while hydroxamate-containing compounds, **18** and **19**, and epoxy ketone **20** exhibited a slow-binding inhibition mechanism for HDAC1, HDAC2, and HDAC3 and lower K_i values (Figure 9). These results indicated that initial K_i values ($K_{i,1}$) determined using dose–response experiments were inappropriate for measuring of the potency of these compounds.
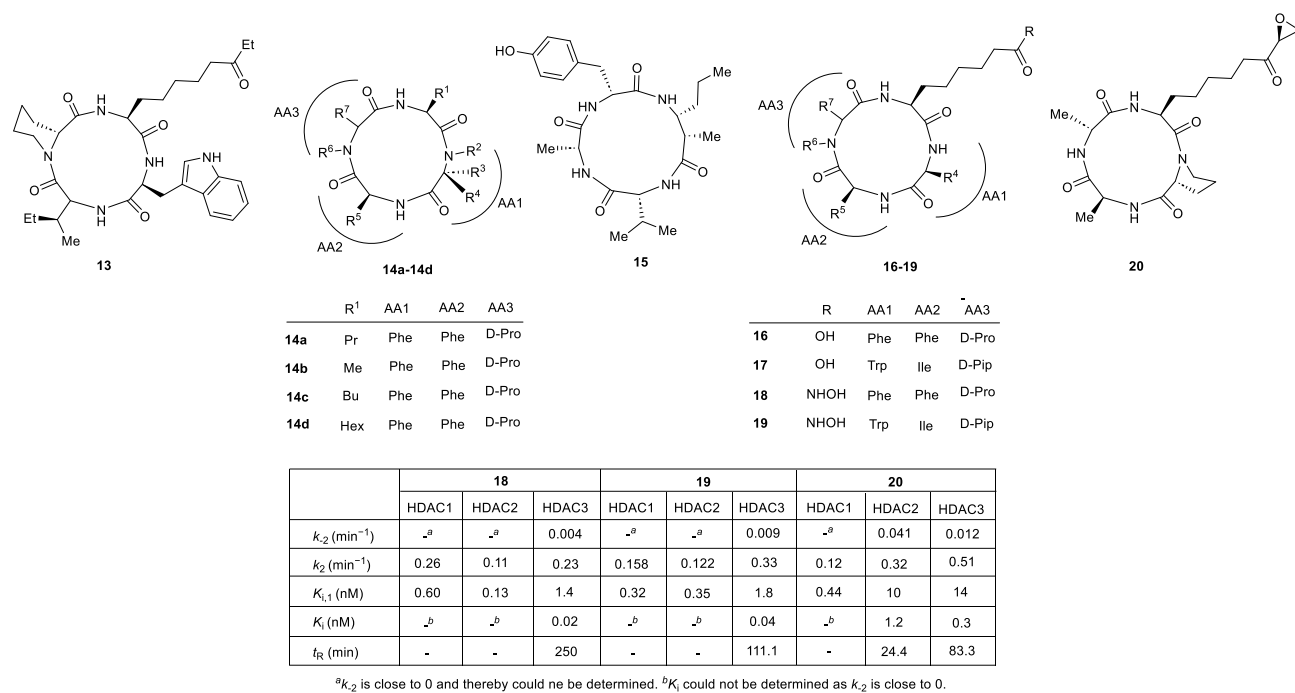

	R^1	AA1	AA2	AA3
14a	Pr	Phe	Phe	D-Pro
14b	Me	Phe	Phe	D-Pro
14c	Bu	Phe	Phe	D-Pro
14d	Hex	Phe	Phe	D-Pro

	R	AA1	AA2	AA3
16	OH	Phe	Phe	D-Pro
17	OH	Trp	Ile	D-Pip
18	NHOH	Phe	Phe	D-Pro
19	NHOH	Trp	Ile	D-Pip

	18			**19**			**20**		
	HDAC1	HDAC2	HDAC3	HDAC1	HDAC2	HDAC3	HDAC1	HDAC2	HDAC3
k_{-2} (min^{-1})	-[a]	-[a]	0.004	-[a]	-[a]	0.009	-[a]	0.041	0.012
k_2 (min^{-1})	0.26	0.11	0.23	0.158	0.122	0.33	0.12	0.32	0.51
$K_{i,1}$ (nM)	0.60	0.13	1.4	0.32	0.35	1.8	0.44	10	14
K_i (nM)	-[b]	-[b]	0.02	-[b]	-[b]	0.04	-[b]	1.2	0.3
t_R (min)	-	-	250	-	-	111.1	-	24.4	83.3

[a]k_{-2} is close to 0 and thereby could ne be determined. [b]K_i could not be determined as k_{-2} is close to 0.

Figure 9. Chemical structures of class I HDAC inhibitors **13**–**20**.

Postmortem studies have revealed that patients who suffered from major depressive disorder, schizophrenia, or bipolar disorder displayed changes in the expression of HDAC1, HDAC2, and HDAC5.[70] Although animal models have suggested that mood disorders and the

HDAC activity are correlated,[71,72] the inhibitors used in these studies exhibited a low specificity for class I HDACs, which can affect other targets in addition to HDACs at high concentrations in the human body. For thoroughly understanding the HDAC inhibition mechanism for the potential application to the treatment of mood disorders, Petryshen *et al.* investigated the impacts of compound **21**, a benzamide-based slow-binding HDAC1/2 inhibitor, on mood-related behavioral assays that usually respond to effective pharmaceuticals (Figure 10).[73] Compound **21** exhibited a selective inhibitory effect on HDAC1 and HDAC2, for which IC_{50} values were 1.0 and 8.0 nM, respectively, and 50- to 400-fold selectivity for HDAC3 (IC_{50} = 458 nM). Additionally, biochemical assays revealed that compound **21** exhibited a strong binding affinity for HDAC1 and HDAC2 (K_i = 0.2–1.5 nM) and slow-on/off kinetics, leading to extended half-lives of 40 and 80 h for HDAC1- and HDAC2-bindings, respectively. Vorinostat, on the other hand, only showed potent inhibitions with modest selectivity for HDAC1, HDAC2, HDAC3, and HDAC6 (IC_{50} = 2.0–11.0 nM) and fast-on/fast-off binding kinetics ($T_{1/2}$ < 4 min for HDAC1-, HDAC2-, HDAC3-bindings). Additionally, in mice, brain pharmacokinetics revealed that compound **21** exhibited a prolonged brain exposure ($T_{1/2}$ = 0.44 and 6.44 h, respectively, for the concentration in the brain) compared with vorinostat. Systematically administered compound **21** showed maximum concentrations in the brain within 5 min, and the concentration remained above 0.1 µM for approximately 8 h. In contrast, although the systemic administration of vorinostat led to rapid peak concentrations, it was eliminated from the brain within 2 h. The administration of slow-binding compound **21** to mice for an extended period caused changes in brain function, which was evident by the altered behavior of the mice in tests for mood-stabilizing and antidepressant drugs. These behavioral changes corresponded to substantial changes in gene expression in those brain regions which are important for regulating mood, including the prefrontal cortex, nucleus accumbens, and hippocampus. However, the administration of fast-binding vorinostat for an extended period

did not affect the mice's mood-related behavior, and the observed transcriptional regulatory changes were different from those produced by compound **21**. Although the systemic administration of vorinostat did not produce any changes in mood-related behavior, previous studies have suggested that the direct infusion of vorinostat into the brain can influence the mood.[74] This suggests that the regulation of the brain neuroplasticity and behavior can both be influenced if HDAC inhibitor concentrations in the brain are sufficiently high. Hence, compared with other fast-binding HDAC inhibitors, slow-binding inhibitors that selectively target HDAC1/2 and exhibit prolonged inhibitory activity may be better therapeutic options in neuropsychiatric disease-treatment models.


21
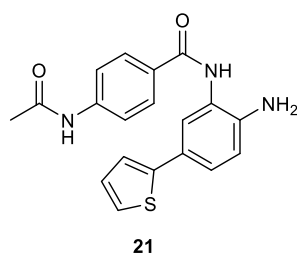
Compound	Kinetic parameter					
	HDAC1		HDAC2		HDAC3	
	K_i (nM)	$T_{1/2}$ (min)	K_i (nM)	$T_{1/2}$ (min)	K_i (nM)	$T_{1/2}$ (min)
Vorinostat	1.9	< 4	15.0	< 4	1.7	< 4
21	< 0.2	> 2400	1.5	> 4800	270	~ 1200

Figure 10. Chemical structure and kinetic parameters of class I HDAC inhibitor **21**.

Compounds featuring a strongly zinc-chelating trifluoromethyl ketone moiety are one of the most studied classes of HDAC inhibitors. In an aqueous solution, trifluoromethyl ketone is easily hydrated and presumably binds to the Zn^{2+} ion in the active site *via* the bidentate coordination of both resulting geminal hydroxy groups.[75,76] Madsen and Olsen studied the inhibitory effects of a known trifluoromethyl ketone compound **22** (Figure 11) on all four HDAC classes. They calculated IC_{50} and K_i values ($K_{i,1}$) using standard endpoint dose–

response assays and found that compound **22** was a class IIa-selective HDAC inhibitor.[13] Initially, a fast-on/fast-off binding mechanism was assumed for compound **22** based on these assays; however, recent studies have suggested that trifluoromethyl ketones may function as slow-binding inhibitors similar to serine protease inhibitors.[77,78] This motivated the authors to reinvestigate the inhibitory mechanism of compound **22** for different HDAC isoforms through a detailed kinetic evaluation. Interestingly, for different class I HDAC isoforms, the inhibition mechanism varied, as shown in Figure 11. When incubated with the class I enzyme, inhibitor **22** showed slow-binding kinetics. The inhibitor showed a competitive slow-binding mechanism (A) (Scheme 1) for HDAC1 and HDAC2, for which K_i was 9.8 and 11.0 μM, respectively. In contrast, compound **22** exhibited a competitive slow-binding inhibitory mechanism (B) (Scheme 1) for HDAC3 and HDAC8 and the longest residence time (t_R = 200 min) on HDAC3, indicating a highly stable enzyme–inhibitor complex. These observations highlight the importance of kinetic assessments for determining the selectivity and performance of inhibitors for various HDAC enzymes.

22
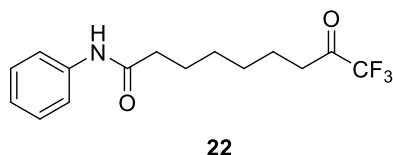
	HDAC1	HDAC2	HDAC3	HDAC8
K_i (nM)	9.8×10^3	1.1×10^4	~11	~33
k_1 (M^{-1} min^{-1})	1.7×10^3	7.7×10^2	-	-
k_{-1} (min^{-1})	1.7×10^{-2}	8×10^{-3}	-	-
$K_{i,1}$ (nM)	-	-	5.7×10^2	7.3×10^3
k_2 (min^{-1})	-	-	0.24	0.49
k_{-2} (min^{-1})	-	-	5×10^{-3}	2.3×10^{-2}
t_R (min)	59	125	200	44

Figure 11. Chemical structure and kinetic parameters of class I HDAC inhibitor **22**.

Dekker *et al.* investigated the kinetic properties of compounds **23**–**25** derived from an HDAC inhibitor, entinostat **26** (Figure 12).[79] Kinetic profiling revealed that although compounds **23** and **24** had slightly higher binding rates than the parent compound **26** on HDAC 1, their k_{on} values were lower than those of compound **26** on HDAC2. Compound **25** had the lowest k_{on} values for HDAC1, HDAC2, and HDAC3 and bound 3.5 times slower than **26** on HDAC3. The dissociation rate constants (k_{off}) of compound **24** were similar for both HDACs 1 and 3. Compound **23** had longer residence times on HDAC1 and HDAC3 (t_R = 14.9 and 10 min, respectively) than compounds **24** and **25**. All the inhibitors showed similar dissociation rates on HDAC2. The researchers used k_{on} and k_{off} ($K_i = k_{off}/k_{on}$) to determine the compounds' affinity rate constants (K_i). All the compounds showed notably different potencies for HDACs 1 and 2 compared with HDAC3, and compound **23** was the most potent inhibitor (K_i = 0.49 µM). Additionally, the authors evaluated the effects of these compounds on both the transcriptional activity and intracellular localization of NF-κB p65 and inflammatory gene expression in LPS/IFNγ-stimulated murine macrophages. Experiments conducted on RAW264.7 macrophages to assess the effect of inhibitors on LPS/IFNγ-induced inflammatory responses revealed that compounds **23** and **25** both suppressed the transcription activity and hindered the nuclear translocation of NF-κB p65. Conversely, compound **24** increased the NF-κB p65 nuclear translocation. Further investigations are required for elucidating the underlying mechanism for the different potencies of HDAC1, HDAC2, and HDAC3 and explaining any related pharmacological distinctions.

Figure 12. Chemical structures and kinetic parameters of class I HDAC inhibitors **23–26**.
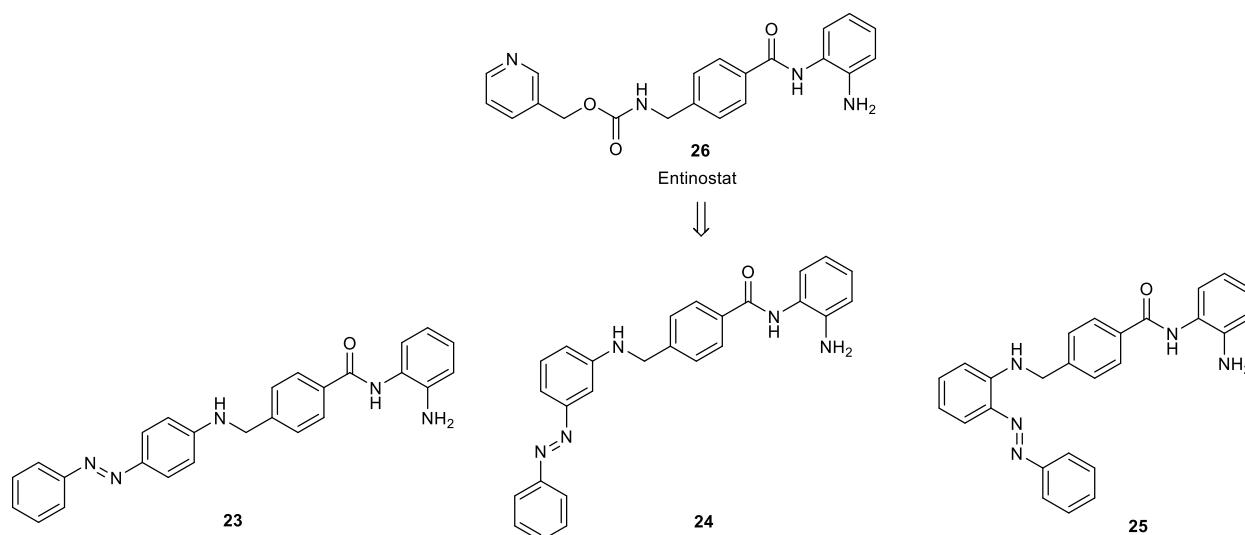
	HDAC1				HDAC2				HDAC3			
	23	**24**	**25**	**26**	**23**	**24**	**25**	**26**	**23**	**24**	**25**	**26**
k_{on} ($\times 10^6$ min^{-1}M^{-1})	0.14	0.17	0.066	0.092	0.073	0.048	0.039	0.10	0.043	0.055	0.017	0.059
k_{off} (min^{-1})	0.067	0.16	0.10	0.076	0.046	0.061	0.064	0.034	0.10	0.14	0.15	0.098
K_i (µM)	0.49	1.0	1.6	0.83	0.63	1.3	1.6	0.33	2.4	2.5	8.7	1.7
t_R (min)	14.9	6.3	10	13.2	21.7	16.4	15.6	29.4	10	7.1	6.7	10.2

Similar to hydroxamate-based inhibitors, such as vorinostat, benzamide-based HDAC inhibitors, such as entinostat **26** (Figure 12), inhibit HDACs by chelating with the zinc ion at the active site. As indicated by their isoform selectivity profiles, these inhibitors reportedly display higher selectivity for class I HDACs.[80,81] However, the exact mechanisms by which these compounds affect biological processes are not fully understood yet. Lauffer *et al.* studied pharmacological inhibition profiles for compound **26**, benzamide derivatives **27** and **28**, and hydroxamate-containing inhibitors vorinostat (Figure 1) and TSA (Figure 13a) for HDACs 1–10.[82] Entinostat **26** showed a submicromolar inhibitory potency for HDAC1, HDAC2, and HDAC3, while, at concentrations between 10 and 50 nM, compounds **27** and **28** selectively inhibited HDAC1 and HDAC2, respectively, without affecting HDAC3. Although the

benzamide and hydroxamate HDAC inhibitors showed relatively similar K_d values, the rate constants (k_{on} and k_{off}) of the benzamide inhibitors **27** and **28** were considerably lower than those of the hydroxamate inhibitors (vorinostat and TSA) by several orders of magnitude (Figure 13a). The vorinostat association and dissociation rates were faster than the assay's detectable limits ($t_R < 1.4$ min), while benzamides **27** and **28** displayed prolonged HDAC1/2 binding kinetics, for which residence times were longer than 20 h. Compounds **27** and **28** both showed residence times that were considerably longer than those of compound **26**, which still dissociated from HDAC1 and HDAC2 more slowly than from TSA. These results were consistent with those for benzamide HDAC inhibitors and hydroxamate pan-inhibitors, which exhibit slow- and rapid-binding kinetics, respectively. The extremely low association and dissociation rate constants for the benzamide inhibitors **27** and **28** suggest that the experimental conditions may have been insufficient for the reactions to equilibrate, which means that IC$_{50}$ values were possibly underestimated. To further investigate the hydroxamate and benzamide inhibitors' binding modes on HDAC2, the authors examined the crystal structures of vorinostat and compound **27** bound to HDAC2 at high resolutions of 1.85 and 1.57 Å, respectively. Structural analysis revealed that the functional groups in both compounds were nearly identically positioned for chelating Zn^{2+} ions in a similar trigonal bipyramidal manner. The structure of the vorinostat–HDAC2 complex showed that the anilide moiety wrapped toward the Phe155 residue, while the alkyl chain spread from the lipophilic channel (Figure 13b(A)). The phenyl ring interacted with the hydrophobic face formed by Phe155 and Pro34 residues, while the amide nitrogen atom formed a polar contact with the Asp104 residue. In contrast, compound **27** exhibited a different binding mode, wherein the thiophene group was in the foot pocket (Figure 13b(B)). At the Leu144 residue, the rotamer flipped, and the Met35 residue shifted by 1 Å, which considerably increased the foot-pocket space. In the thiophene moiety, the 2- and 5-positions showed a higher electron density, suggesting that the ring can flip and

the sulfur atom can fit both orientations. This protein rearrangement to generate the foot pocket and requirement for a hydrogen bond to rupture within the ligand upon binding are consistent with the slower binding kinetics of benzamide inhibitors compared with those of hydroxamate inhibitors. When the ligand approaches the protein molecule, the hydroxamate moiety interacts with the catalytic zinc ion at the base of a hydrophobic tube by displacing bound water molecules, which means that hydroxamate-containing ligands typically have fast-binding kinetics. Benzamides, on the other hand, reach the binding mode through a more-challenging path *via* two potential binding approaches based on substantial protein rearrangement. Benzamides can enter through an acetyl release and disposal channel or a hydrophobic tube and insert into a rearranged foot pocket before forming the zinc complex, which locks the inhibitor in place. This is consistent with the slow-binding kinetics of benzamide compounds **27** and **28**. Using these kinetic parameters, the authors then investigated the effects of hydroxamate and benzamide kinetics on the abilities of hydroxamate and benzamide to modify the histone acetylation in SH-SY5Y neuroblastoma cells. In cell-based assays, both HDAC inhibitors considerably increased the histone acetylation level. Compared with vehicle-treated controls, inhibitor-treated cells showed considerably higher H2BK5 and H4K12 acetylation levels, which were then used as markers to assess the long-term effects of benzamide or hydroxamate HDAC inhibitors. For both markers, vorinostat- and TSA-treated cells both exhibited a rapid acetylation onset, wherein the levels were maximized by 6 h and diminished until they were barely detectable at 96 h. However, for H2BK5 and H4K12, compounds **26**–**28** delayed the hyperacetylation onset; the levels were maximized between 24 and 48 h and only declined after 96 h, which suggests that the acetylation magnitude indicates the difference in the inhibitor selectivity because hydroxamates inhibit more HDAC isoforms than benzamides. Additionally, the authors pulsed the inhibitors for 6 h, washed the cells, replaced the inhibitor-free media, and then monitored the hyperacetylation from 0 to 96 h. For the

hydroxamate inhibitors (vorinostat and TSA), incubation 6 h considerably increased the acetylation at both measured markers and then returned to the baseline within 18 h after drug-free media were added. However, although compounds **26–28** elevated the histone acetylation that had been continuously exposed for the same period, the histone deacetylation was considerably delayed after the inhibitor was washed out. Even after 96 h, the acetylation levels did not return to their baseline. These observations provide evidence that hydroxamates' high kinetic rates and benzamides' slow-binding characteristics both affect the histone acetylation and deacetylation in different manners after compounds are added and removed, respectively.

(a)
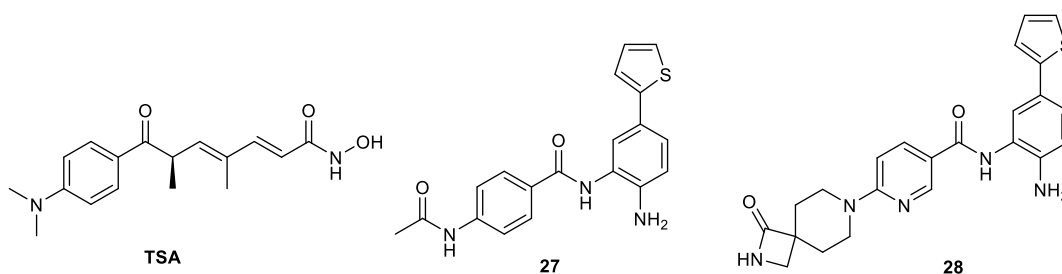
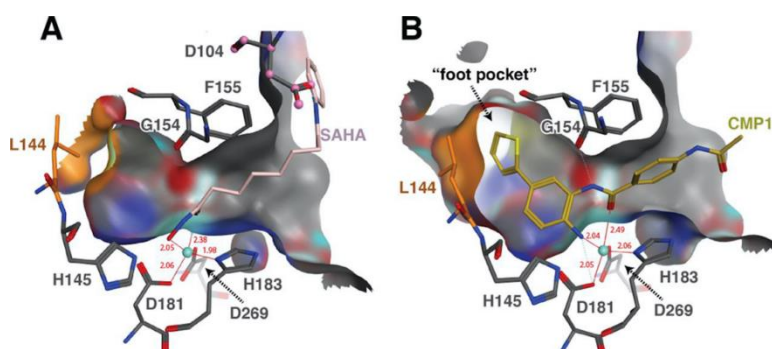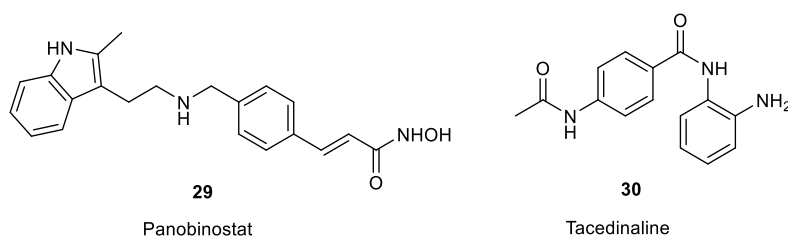|	HDAC1					HDAC2				
	26	**27**	**28**	**TSA**	**Vorinostat**	**26**	**27**	**28**	**TSA**	**Vorinostat**
k_{on} (min^{-1}M^{-1})	2.66×10^4	2.09×10^4	2.4×10^4	2.77×10^6	-	8.63×10^3	1.50×10^4	9.01×10^3	3.64×10^6	-
k_{off} (min^{-1})	7.50×10^{-3}	7.94×10^{-4}	5.91×10^{-4}	3.35×10^{-2}	-	1.35×10^{-3}	8.28×10^{-4}	4.33×10^{-4}	5.59×10^{-2}	-
K_d (µM)	0.282	0.0381	0.0246	0.0121	0.163	0.156	0.0552	0.0481	0.0153	0.182
t_R (min)	133	1259	1692	30	<1.4	743	1207	2309	18	<1.4

(b)

Figure 13. (a) Chemical structures and kinetic parameters of class I HDAC inhibitors **27** and **28**; A comparison of the structural analysis of vorinostat and compound **27** binding to HDAC2. Interior views of the binding pocket for vorinostat bound to HDAC2 (A) and compound **27** bound to HDAC2 (B). The binding pocket surface is depicted in gray, SAHA and compound **27** are represented as pink or gold stick models, respectively. The zinc ion is shown as a turquoise sphere, and key HDAC2 pocket residues are displayed as gray sticks. Leucine 144, which alters rotamers to open the foot pocket, is depicted in orange sticks. Reproduced with permission from [82]. Copyright [2013] [American Society for Biochemistry and Molecular Biology].

Frontotemporal dementia (FTD), the second most frequently occurring type of presenile dementia, is caused by the haploinsufficiency of the progranulin gene (GRN) and reduced progranulin (PGRN) expression. FTD affects 10–15 per 100,000 adults aged between 45 and 65 years.[83] The improvement of the GRN gene expression by inhibiting HDAC1, HDAC2, and HDAC3 is a promising strategy for rescuing the haploinsufficient FTD phenotype.[84] Recent studies have shown that although not all HDAC1–3 inhibitors can increase the PGRN expression in human neuron models, they exhibit a high inhibitory potency for the overall histone hyperacetylation in the same cell lines.[85] Although the mechanisms through which HDAC inhibition regulates the GRN in neurons remain poorly understood, the binding kinetics of HDAC inhibitors seem to play a critical role. In theory, to affect both the HDAC acetylation and GRN regulation, the HDAC inhibitor must bind quicker than the HDAC–chromatin associates with the GRN promoter.[85] Accordingly, slow-binding inhibitors, which follow mechanism B (Scheme 1), should be more efficient for enhancing the PGRN expression because the extended residence time on the HDAC is believed to be another key factor for inducing the PGRN expression. In a recent study, the effects of selective HDAC1–3 inhibitor families, namely, panobinostat **29**, tacedinaline **30**, and peptide-based macrocyclic romidepsin **12** (Figures 8 and 14), on both HDAC acetylation and PGRN expression were tested in human iPSC-derived neural progenitor cells.[86] All the inhibitors exhibited high inhibitory activity for the deacetylation of acetylated H3K9. However, despite their slow-binding inhibition behavior, all the compounds had markedly different effects on the PGRN level. The hydroxamic-acid-based compound **29** is strongly bound to HDAC1–3, and its action against HDAC2 was nearly irreversible and had a long half-life ($T_{1/2} > 10^5$ min). This property may guide the development

of PGRN enhancers exhibiting prolonged and improved pharmacological effects without the need for an *o*-aminoanilide component to prolong the binding kinetics. Peptide-based macrocyclic romidepsin **12** exhibited a potent inhibition for HDAC1, HDAC2, and HDAC3 and an extended half-life ($T_{1/2} > 10^5$ min) on HDAC3. Additionally, tacedinaline **30**, a member of the benzamide HDAC1–3 inhibitor family, exhibited a slow-binding inhibition through mechanism B (Scheme 1), with nanomolar potencies and prolonged residence times on HDAC1, HDAC2, and HDAC3. However, although **30** increased the H3 acetylation by 18-fold at a similar concentration, it did not alter PGRN levels. In contrast, the hydroxamic acid-based compound **29**, which had a similar effect on the H3 acetylation (increased by ~36-fold), also showed prolonged residence times and potent inhibitions for HDAC1, HDAC2, and HDAC3 without requiring a benzamide component (Figure 14). Previous studies have suggested that only benzamide HDAC inhibitors do not exhibit a correlation between the HDAC inhibition and PGRN expression,[85] which indicates that further research is required for determining the accurate mechanism through which HDAC inhibitors promote the upregulation of the PGRN.
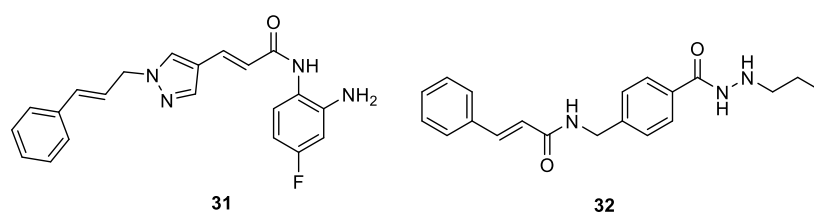
	29			12			30		
	HDAC1	HDAC2	HDAC3	HDAC1	HDAC2	HDAC3	HDAC1	HDAC2	HDAC3
k_{-2} (min^{-1})	1.7×10^{-2}	1×10^{-12}	1.1×10^{-2}	2.7×10^{-2}	1.7×10^{-2}	-	5×10^{-4}	5×10^{-3}	1.4×10^{-2}
k_2 (min^{-1})	4.9	1.2	1.7	1.14	0.88	0.47	0.84	0.80	0.46
$K_{i,1}$ (nM)[a]	33	4.7	15	0.88	0.47	1.3	1450	2190	3560
K_i (nM)	~0.1	-[b]	0.1	~0.02	0.009	-[b]	~1	~14	105
$T_{1/2}$ (min)[c]	≥ 41	> 10^5	≥ 63	≥ 26	≥ 41	> 10^5	≥ 1386	≥ 139	≥ 50
t_R (min)	59	10^{12}	91	37	59	-	2000	200	71
PGRN level Ac H3K9 level[d]	~2.3-fold increase ~36-fold increase			~4.1-fold increase ~2.3-fold increase			- ~18-fold increase		

[a]Mechanism B in Scheme 1. [b]K_i could not be determined as k_{-2} is close to 0. [c]Dissociative half-life of inhibitor-HDAC complex. [d]NPCs incubated with 1 µM of inhibitor.

Figure 14. Kinetic parameters and biological activity of class I HDAC inhibitors panobinostat **29**, romidepsin **12**, and tacedinaline **30**.

Moreno–Yruela and Olsen utilized both continuous and discontinuous assays to investigate the potency and selectivity of slow-binding inhibitors **31** and **32**.[87] When an HDAC isoform was simultaneously incubated with an inhibitor and a substrate (preincubated for 0 h), compounds **31** and **32** both selectively inhibited HDAC3 compared with HDAC1 and HDAC2 (Figure 15). Because slow-binding inhibitors, such as benzamide- and acyl hydrazide-based inhibitors, usually require more than 30 min to equilibrate, the authors preincubated the enzyme and inhibitor for various periods (30 min, 1 h, and 2 h) before adding the substrate to analyze the kinetic profiles of inhibitors **31** and **32**. Endpoint assays revealed that compound **31** could equilibrate the enzyme–inhibitor complex in 0–30 min with only slightly different IC$_{50}$ values. Compound **32**, on the other hand, considerably reduced IC$_{50}$ values when it was preincubated with HDAC1 and HDAC2, indicating a slow-binding characteristic. Preincubation decreased the HDAC3-selectivity of compound **32** while retaining the compound's potency against

HDAC3. When the discontinuous assay system was changed to a continuous assay system, the enzyme kinetics revealed that **31** and **32** were slow-binding inhibitors of HDAC1, HDAC2, HDAC3. Compound **32** inhibited HDAC1 and HDAC2 through a slow-binding mechanism (A) and HDAC3 through mechanism B (Scheme 1). Compound **31**, initially thought to inhibit HDAC3 selectively, was recognized as a slow-binding inhibitor for HDAC1, HDAC2, HDAC3, for which K_i value were 57, 31, and 13 nM, respectively. These results highlight the importance for comprehensively analyzing kinetics for precisely determining the isoform selectivity of slow-binding inhibitors targeting HDACs.

preincubation		**31**			**32**		
		HDAC1	HDAC2	HDAC3	HDAC1	HDAC2	HDAC3
	0 h	2.66 µM	1.63 µM	0.51 µM	36.4 nM	89.9 nM	5.96 nM
IC$_{50}$	0.5 h	3.73 µM	2.85 µM	1.24 µM	11.3 nM	48.0 nM	8.2 nM
	1 h	4.66 µM	3.35 µM	1.06 µM	7.07 nM	24.8 nM	7.84 nM
	2 h	6.0 µM	2.74 µM	1.61 µM	4.89 nM	14.0 nM	10.2 nM

	31			**32**		
	HDAC1	HDAC2	HDAC3	HDAC1	HDAC2	HDAC3
k_1 (nM^{-1}min^{-1})	-	-	-	7.8×10^{-5}	5.1×10^{-5}	-
k_{-1} (min^{-1})	-	-	-	3×10^{-3}	5×10^{-3}	-
k_2 (min^{-1})	0.4	0.38	0.3	-	-	0.78
k_{-2} (min^{-1})	2×10^{-2}	7×10^{-3}	5×10^{-3}	-	-	4×10^{-11}
$K_{i,1}$ (nM)	1300	1700	700	-	-	25
K_i (nM)	57	31	13	40	103	-[a]
$T_{1/2}$ (min)[b]	≥36	≥95	≥131	220	130	$<10^5$
t_R (min)	50	143	200	-	-	2.5×10^{10}

[a]K_i could not be determined as k_{-2} is close to 0. [b]Dissociative half-life of inhibitor-HDAC complex.

Figure 15. Chemical structures and kinetic parameters of class I HDAC inhibitors **31** and **32**.

At the long terminal repeating unit of HIV-1, the HDAC-induced histone deacetylation can both repress the transcription and establish the viral latency, which suggests that HDAC inhibitors could be an option for eradicating persistent and dormant HIV-1 proviral infections. HDAC3 inhibition is the key for activating latent HIV-1.[88] Liu *et al.* employed a parallel medicinal chemistry strategy utilizing 2-substituted benzamide as the ZBG to identify HDAC 3-selective inhibitors (Figure 16).[89] Their investigations revealed that compound **33** strongly inhibited HDAC3 (IC_{50} = 29 nM) exhibited 690- and 1,069-fold selectivity over HDACs 1 and 2 (IC_{50} = 20 and 31 μM), respectively. Additionally, compound **33** showed a slow-binding behavior on HDAC3, as evidenced by its associated on and off rates ($1.5 \times 10^4 \, M^{-1} \, s^{-1}$ and $4.4 \times 10^{-4} \, s^{-1}$, respectively) and a residence time (t_R) of 0.63 h. However, **33** exhibited a potent hERG binding activity, for which IC_{50} was 16 nM. Nevertheless, compounds **34** and **35** were developed by slightly modifying the imidazole core and exhibited reduced off-target effects on hERG, for which IC_{50} values were 1.33 and 13 μM, respectively. Furthermore, a slight alteration from 2-methylthio to 2-hydroxy benzamide in compound **36** preserved the compound's HDAC3 potency while eliminating the compound's selectivity over HDACs 1 and 2. Although inhibitor **36** exhibited a high on-rate for HDAC3, this rate was still lower than that of compound **33**. Notably, for compound **33**, the off-rate for HDAC3 was calculated at $4.0 \times 10^{-6} \, s^{-1}$, which means that the residence time (t_R = 69.4 h) was much longer than that of compound **33**. This suggests that the selectivity of inhibitor **33** is due to the monodentate coordination of the 2-substituted methylthiophenyl group with the zinc ion, which induces the flipping of the Tyr305 residue's side chain and stabilizes the binding pocket through the formation of the HDAC3/IP4/SMRT complex.

Figure 16. Chemical structures, kinetic parameters, and hERG-inhibitory activity of class I HDAC inhibitors 33–36.
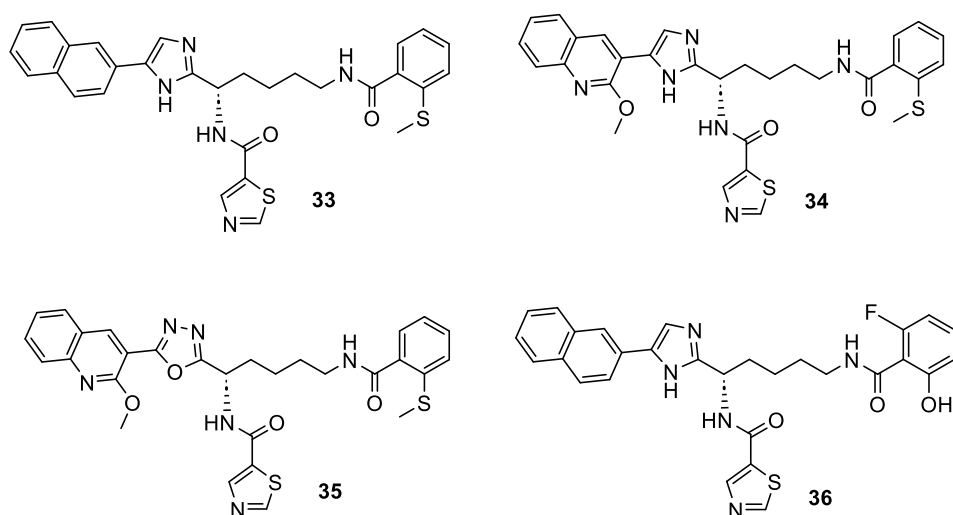
Compound	IC$_{50}$			k_{on} (M^{-1}s^{-1})	k_{off} (s^{-1})	t_R (h)	hERG IC$_{50}$
	HDAC1	HDAC2	HDAC3				
33	20 µM	31 µM	29 nM	1.5 × 10^4	4.4 × 10^{-4}	0.63	16 nM
34	>45 µM	>45 µM	114 nM	-	-	-	1.33 µM
35	>45 µM	>45 µM	857 nM	-	-	-	13 µM
36	9.7 nM	29 nM	7.6 nM	1.7 × 10^3	4.0 × 10^{-6}	69.4	-

Zhang *et al.* developed a method and proposed a mechanism for identifying chalcone-based inhibitors **37** and **38** (Figure 17a), which selectively target HDAC1 and HDAC2 more than HDAC3.[90] The selectivity of β-substituted chalcones for HDAC1 and HDAC2 appears to be due to the steric hindrance in the binding pocket, which is less pronounced in HDAC3 than in both HDAC1 and HDAC2. As depicted in Figure 17b, HDAC3 readily accommodates the benzamide segment. However, to accommodate the extended B ring of the β-hydroxymethyl-chalcone, Tyr96 in HDAC3 needs to be rotated outward, indicating the presence of steric effects in the binding site. In contrast, HDAC1/2, with a larger foot pocket, can easily accommodate the extended B-ring of the β-substituted chalcone without altering the side chain orientation of Ser113/118. These computational observations supported the steric hindrance hypothesis. The preincubation of inhibitor **37** with HDAC2 for different periods considerably

decreased IC_{50} from 9.19 to 0.17 μM, which enhanced the selective inhibition of HDAC2 by 54-fold (Figure 17a). This time-dependent inhibition through a slow-binding mechanism was thought to control the selective inhibition of HDAC2 more than that of HDAC1. The authors proposed that the underlying mechanisms for the distinct kinetic isoform selectivity of the β-hydroxymethyl chalcone **37** for HDAC2 were related to the period that the inhibitor remained bound to the target, hydrogen bond alternations, and local conformational changes that occur during the formation of the enzyme–inhibitor complex. Although HDAC1/2 share a highly similar pocket shape and conserved residues around the active site, it would be expected that two β-substituted chalcones yield similar binding kinetics towards either HDAC1 or HDAC2. However, experimental results indicated that only the β-hydroxymethyl chalcone **37** shows distinct and unique slow-binding kinetics on HDAC2, while no time-dependent effect is observed for β-aminomethyl chalcone **38** towards either HDAC1 or HDAC2. The authors proposed a contributing factor termed the "tandem reaction time-dependent tight-binding kinetics" mechanism, based on the subsequent dynamic equilibrium of the intramolecular nucleophilic attack reaction (formation of [E•I]′) (Figure 17c). This mechanism explains the observed distinct time-dependent inhibition of β-hydroxymethyl chalcone **37** towards HDAC2. The researchers hypothesized that this discrepancy was due to the intramolecular nucleophilic attack of the hydroxy group on the carbonyl group and found that for HDAC2, the energy barrier for this reaction was considerably lower for inhibitor **37** than for inhibitor **38** (14.6 and 23.7 kcal/mol, respectively) (Figure 17a), which could be because the Ca^{2+} ion is approximately 7 Å from the catalytic Zn^{2+} ion in HDAC2. The Ca^{2+} ion could remotely increase the charge on the catalytic Zn^{2+} ion and act as a stronger Lewis acid to promote the intramolecular nucleophilic attack reaction. This selective mechanism may contribute to the slow-binding kinetics of HDAC2.

(a)

Compound	IC$_{50}$ (μM)						Energy barrier^a (kcal mol^{-1})	
	HDAC1		HDAC2		HDAC3		HDAC1	HDAC2
	1 h	24 h	1 h	24 h	1 h	24 h		
37	3.68	2.74	9.19	0.17	~50	~50	21.2	14.6
38	5.96	8.65	19.64	26.44	>50	>50	27.7	23.7

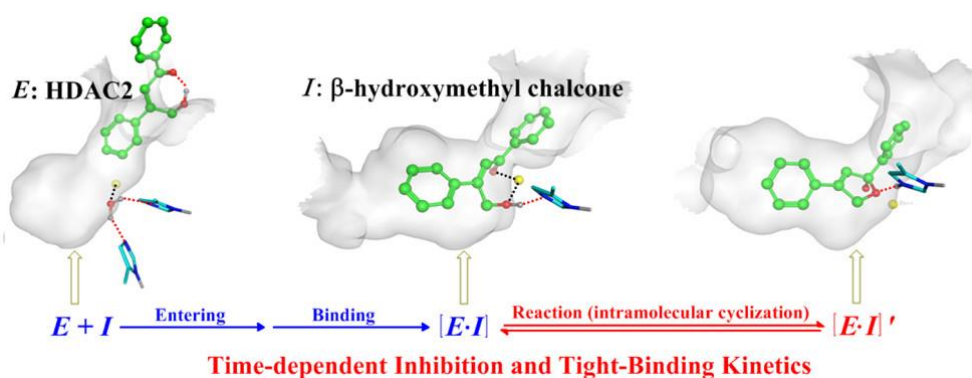^{a}Energy barrier for the intramolecular nucleophilic attack reaction between HDAC and inhibitor.

(b)
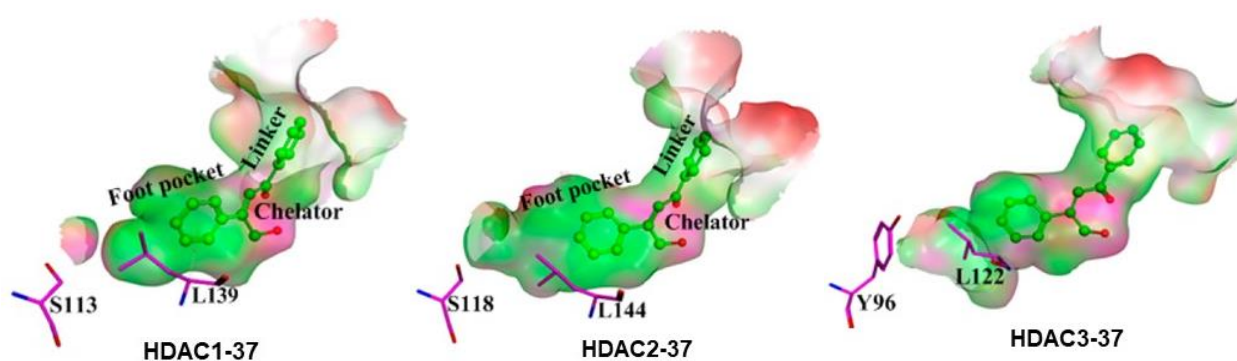
(C)

Figure 17. (a) Chemical structures, IC$_{50}$ values, and energy barriers for intramolecular nucleophilic reaction of class I HDAC inhibitors **37** and **38**; (b) Binding of inhibitor **37** in the active pocket of HDACs1, 2, and 3, respectively, where red indicates the exposed region, pink represents the polar region, and green designates the hydrophobic region. Reproduced from [90]. Copyright [2015] [American Chemical Society]; (c) Proposed key factors of time-dependent tight-binding kinetics of HDAC inhibitors **37** and **38**. Reproduced from [90]. Copyright [2015] [American Chemical Society].

Although numerous attempts have been made to discover potent HDAC inhibitors for treating lymphoma and myeloma, the number of approved inhibitors remains limited. Because currently approved inhibitors have hydroxamate (vorinostat and belinostat) or thiolate

40

(romidepsin) as the ZBG,[91] Chou *et al.* aimed to find selective HDAC inhibitors containing a different ZBG. They developed compounds **40** and **41**,[92] which contained a hydrazide ZBG, based on their previously reported class I selective inhibitor **39** (Figure 18).[93] Although inhibitor **40** initially showed potent activity against class I HDACs, the preincubation of inhibitor **40** with HDAC1, HDAC2, and HDAC3 for 15–90 min considerably reduced IC_{50}, which suggested that a slow-binding inhibition was involved for class I HDACs (Figure 18). Furthermore, the optimization of the linkers in inhibitor **40** led to the development of inhibitor **41**, which showed lower IC_{50} values (9.54, 28.04, and 1.41 nM for HDAC1, HDAC2, and HDAC3, respectively) and was more potent than inhibitor **40** against MV4-11 cells. The response to inhibitor **41** varied depending on the cell type. Inhibitor **41** induced apoptosis in p53 wild-type IV4-11 cells and arrested G2/M, which had a cytostatic effect in p53-null PC-3 cells.
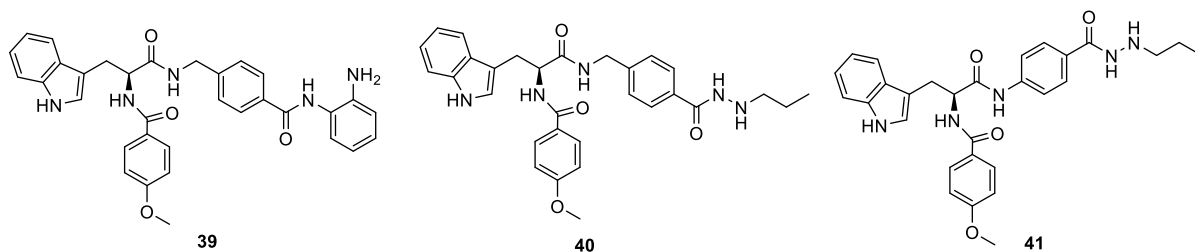
Compound	IC_{50} (nM)											
	HDAC1				HDAC2				HDAC3			
	15 min	30 min	6 0min	90 min	15 min	30 min	60 min	90 min	15 min	30 min	60 min	90 min
39	99.9	64.9	49.8	34.5	347.9	252.4	168.8	121.3	938.5	433.0	183.8	134.7
40	91.2	77.5	50.1	32.9	423.7	366.9	259.9	194.0	17.9	14.4	8.5	5.7

Figure 18. Chemical structures and time-dependent inhibitory effects of class I HDAC inhibitors **39**–**41**.

Chou *et al.* subsequently developed another hydrazide-based inhibitor **42** (Figure 19), which showed potent inhibitory effects against HDAC1, HDAC2, and HDAC3, for which IC_{50} values were 5.17, 49.5, and 0.28 nM, respectively.[94] The preincubation of HDAC1 and HDAC3

with inhibitor **42** for 10, 30, 60, or 90 min considerably reduced the corresponding IC$_{50}$ values, which indicates a slow-binding mechanism against class I HDACs (Figure 19). A western blot analysis revealed that the prolonged histone acetylation persisted for up to 6 h after inhibitor **42** was removed from the MV4-11 cells, which suggested that a low off-rate and an enhanced drug–target residence time both contributed to the inhibitor's isoform selectivity. Additionally, inhibitor **42** indirectly downregulated FLT3, pERK, and STAT5, which inhibit the FLT3 signaling pathway in wild-type p-53 FLT3-ITD MV4-11 cells. This indicates the potential of inhibitor **42** for treating acute myelogenous leukemia exhibiting the FLT3 mutation.
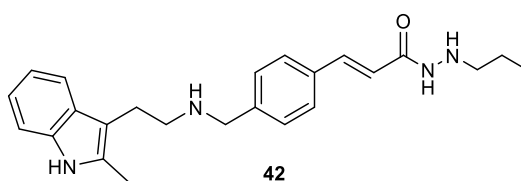
IC$_{50}$ (nM)							
HDAC1				HDAC3			
10 min	30 min	60 min	90 min	10 min	30 min	60 min	90 min
17.35	12.30	9.64	6.46	0.53	0.32	0.26	0.17

Figure 19. Chemical structure and time-dependent inhibitory effect of class I HDAC inhibitor **42**.

Mai *et al.* addressed the rapid metabolism of hydroxamate-based HDAC inhibitors by developing a 9-substituted purine-based aminobenzamide **43** (Figure 20).[95] This inhibitor has a 12-fold higher potency than entinostat, an IC$_{50}$ value of 55.1 nM for HDAC1, and improved metabolic stability compared with that of vorinostat. In HCT-116 cells, inhibitor **43** induced a dose-dependent increase in H3K9 and H4K5 acetylation levels, which persisted for up to 48 h. In contrast, vorinostat rapidly increased H3K9 and H4K5 acetylation levels, which returned to the baseline in 12 h. This indicates that inhibitor **43** exhibits a slow-binding mechanism.
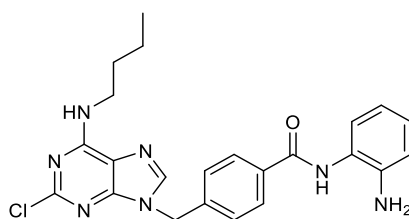
43

Figure 20. Chemical structure of class I HDAC inhibitor **43**.

Various ZBGs, such as benzamides, hydrazides, and hydroxamates, have been incorporated into numerous HDAC inhibitors. However, the understanding of how these ZBGs impact both the potency and isoform selectivity is limited.[96] Therefore, Li *et al.* modified the hydroxamate moiety in vorinostat to benzamide and hydrazide moieties without changing the linker or capping group[97] to investigate how these changes affected both the potency and isoform selectivity. To assess their enzymatic profiles, compounds **44a** and **44b** (Figure 21) were then evaluated against HDACs. In contrast to vorinostat, these compounds had a selective inhibitory effect on class I HDACs, for which compound **44b** exhibited a considerably higher inhibitory potency than **44a**. A dose–response analysis conducted at different time intervals revealed that compound **44b** exhibited a 3-fold higher potency when preincubated with HDAC1 for 120 min compared to only 5 min, for which IC_{50} values were 175.6 and 48.4 nM, respectively (Figure 21). These results suggested that the inhibitor was slowly released from the enzyme and engaged its target more easily. In contrast, compound **44a** displayed a fast-on inhibition, which is unusual for benzamide-based inhibitors that have slow-binding kinetics. These results indicate that the slow-binding profile is not only exclusively attributed to the ZBG but also influenced by both the cap and linker groups.
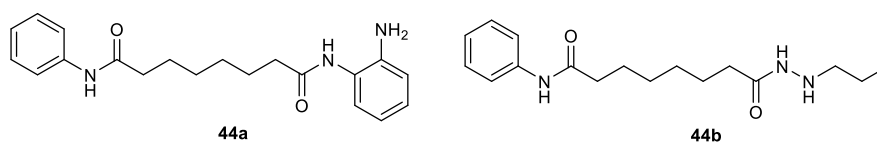
Compound	IC$_{50}$ (nM)														
	HDAC1					HDAC2					HDAC3				
	5 min	30 min	60 min	90 min	120 min	5 min	30 min	60 min	90 min	120 min	5 min	30 min	60 min	90 min	120 min
44a	944.2	910.1	1135	1217	1066	1156	1166	1170	1356	1272	658.7	558.7	535.3	391.4	463
44b	175.6	89.21	62.94	41.85	48.4	405.8	303.7	214	162.8	145.6	58.24	30.14	22.88	17.19	17.72

Figure 21. Chemical structures and time-dependent inhibitory effects of class I HDAC inhibitors **44a** and **44b**.

Recently, Suzuki *et al.* developed a small molecule, KTT-1 **45** (Figure 22a) as a kinetically HDAC2-selective inhibitor.[98] Compared with HDAC1, HDAC2 exhibits a longer KTT-1 residence time (t_R = 3330 and 145 min for HDAC2 and HDAC1, respectively), which indicates a 23-fold kinetic selectivity for HDAC2 over HDAC1. To investigate the underlying cause of kinetic selectivity of **45** towards HDAC2, a cocrystal structure of HDAC2 bound to **45** was solved (Figure 22b(A)). Despite having this structural information, understanding the physical basis for the kinetic selectivity of the inhibitor remained challenging. Recognizing that the residence time of an inhibitor is determined by the association and dissociation energies between the inhibitor and its target enzyme, the researchers needed to consider the dynamic structural properties of the system to gain deeper insights. These dynamic properties are crucial for comprehending the time-dependent interactions between **45** and HDAC2, which ultimately contribute to the observed kinetic selectivity. For comprehensively investigating the physical basis of this kinetic selectivity, the authors utilized advanced molecular dynamics simulations *via* replica-exchange umbrella sampling.[10] Using this method, the authors meticulously investigated the formation of both **45**:HDAC2 and **45**:HDAC1 complexes and found that although **45** formed a highly stable interaction with HDAC2, it readily dissociated from HDAC1. By analyzing the immediate vicinity of the binding site in HDAC1 and HDAC2, the

researchers found a conserved loop containing four consecutive glycine residues (Gly304–307 and Gly299–302 in HDAC2 and HDAC1, respectively) that were involved in the kinetic selectivity of HDAC2. The distribution analysis revealed that the three atoms including C^β of Ser263, C^α of Gly301, and C3 of **45** are arranged in a non-linear manner (Figure 22b(B)). On the other hand, the three atoms of C^β of Ala268, C^α of Gly306, and C3 of **45** in HDAC2 form a linear arrangement (Figure 22b(C)). This difference in orientation has important implications for the binding of KTT-1 to HDAC1 and HDAC2. It was proposed that the linear orientation of the three atoms in HDAC2, particularly the C^β of Ala268, indirectly contributes to the tight binding of **45**. This linear arrangement allows for consistent and favorable forces to act from the C^β of Ala268 to the C^α of Gly306 and from the C^α of Gly306 to the C3 of **45**, promoting stable binding. In contrast, the non-linear orientation of the three atoms in HDAC1, especially the C^β of Ser263, prevents effective stabilization of **45** binding. The slightly greater distance between the C^β of Ser263 and the C^α of Gly301, along with the non-linear orientation, results in different directions of forces acting from the C^β of Ser263 to the C^α of Gly301 and from the C^α of Gly301 to the C3 of **45**, making the binding less stable. The tight fitting of the glycine loop between Ala268 in HDAC2 and **45** further supports the favorable binding in HDAC2. However, the glycine loop cannot achieve a tight fit with Ser263 in HDAC1 and **45** due to the non-linear arrangement, contributing to the weaker binding in HDAC1. These findings provide insight into the intricate molecular interactions that drive the mechanism through which compound **45** selectively inhibits HDAC2 more than HDAC1.
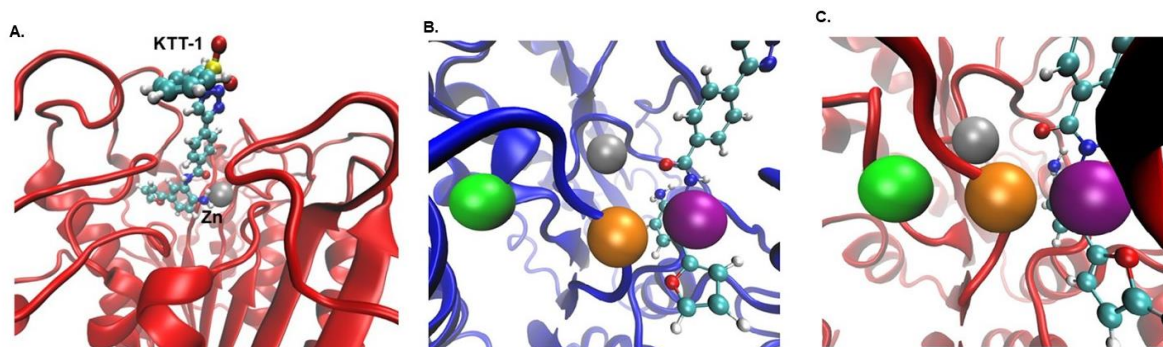
(a)

45
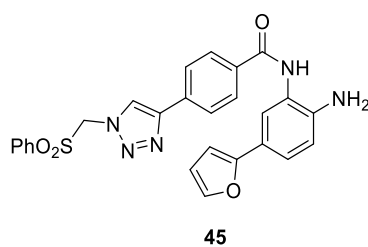
(b)

Figure 22a. (a) Chemical structures of class I HDAC inhibitor **45** (KTT-1); (A) The cocrystal structure of inhibitor **45** (KTT-1) and HDAC2. (B) Interaction of inhibitor **45** at the catalytic site of HDAC1. (C) Interaction of inhibitor **45** at the catalytic site of HDAC2. The green, orange, and purple spheres are the C^β atom of Ser263/Ala268, the C^α atom of Gly301/306, and C3 of inhibitor **45**, respectively. Reproduced with permission from [10]. Copyright [2023] [Wiley-VCH].

Liao *et al.* reported a new class I selective HDAC inhibitor **46** bearing benzoylhydrazide moiety with IC_{50} values of 500 nM, 100 nM and 60 nM against HDACs1, 2, and 3, respectively (Figure 23).[99] This targeted inhibition resulted in notable changes in protein acetylation and gene expression, culminating in the activation of tumor suppressor pathways and the simultaneous inhibition of multiple oncogenic pathways. These findings underscore the potential of inhibitor **46** as a promising therapeutic candidate for combating cancer growth and progression. Interestingly the inhibition kinetic experiment using HCT116 cells revealed that upon treatment with inhibitor **46**, a swift increase in histone acetylation was detected within 6 h, and these elevated acetylation levels persisted for up to 96 h. These findings suggested that inhibitor **46** functions as a fast-on but slow-off inhibitor, showcasing its capacity to effectively regulate histone acetylation dynamics with prolonged residence time.
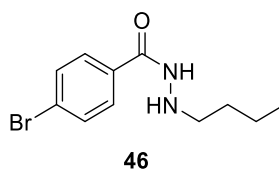
46

Figure 23. Chemical structures of class I HDAC inhibitor **46**.

Hansen *et al.* identified a novel inhibitor, compound **47**, based on the *o*-aminoanilide structure (Figure 24a).[100] This inhibitor demonstrated a selective affinity for the "foot-pocket" region within both HDAC1 and HDAC2 enzymes. To gain a deeper insight into the potential binding mode of the inhibitor, the authors performed a docking analysis of compound **47** within the structure of HDAC1 (PDB: 5ICN), as depicted in Figure 24b. The docking results revealed that the zinc-binding takes place through the *o*-aminoanilide moiety of compound **47**. Additionally, the 4-pyridinyl-group of compound **47** was found to significantly interact with the distinct "foot-pocket" region of HDAC1, further confirming its targeted binding mode. Furthermore, inhibitor **47** exhibited a hydrogen-bond interaction between the side chain of Y296 and the amide NH group of the zinc-binding group (ZBG). This specific interaction adds to the understanding of the molecular interactions contributing to the binding affinity of compound **47** within HDAC1's active site. When subjected to varying preincubation durations of 5, 15, 30, 60, and 120 minutes, compound **47** exhibited a noticeable reduction in its IC_{50} values for HDAC1 and HDAC2 (Figure 24a). Intriguingly, this time-dependent decrease in inhibitory potency was not observed in the case of HDAC3, suggesting a unique and distinct slow-binding inhibitory effect specifically targeting HDAC1 and HDAC2. Further investigations utilizing the WST-8 assay within three different breast cancer cell lines including T-47D, MCF-7, and BT-474 revealed that the antiproliferative properties of compound **47** were notably more impressive compared to those of entinostat and vorinostat.

(a)

47
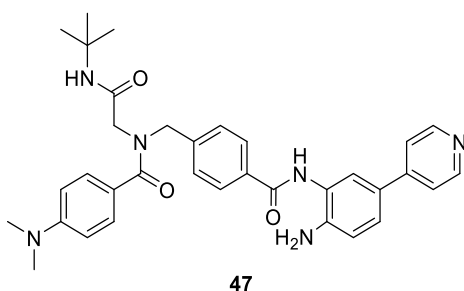
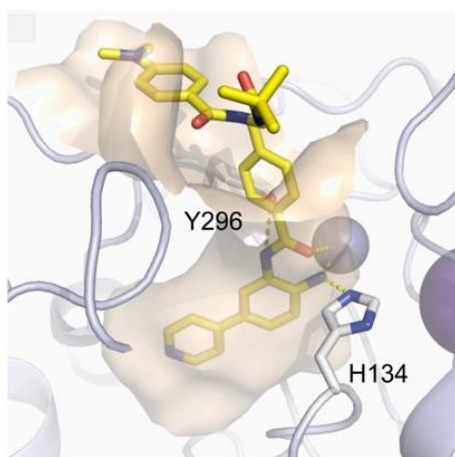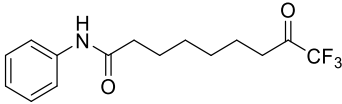| Compound	IC$_{50}$ (nM)									
	HDAC1					HDAC2				
	5 min	15 min	30 min	60 min	120 min	5 min	15 min	30 min	60 min	120 min
47	53.0	48.9	34.7	27.9	20.7	117.4	106.4	109.0	84.0	78.1

(b)

Figure 24. (a) Chemical structure and time dependent inhibitory effect of class I HDAC inhibitor **47**; (b) Docking pose of inhibitor **47** in the catalytic domain of HDAC1 (PDB: 5ICN). Ligands are shaded in yellow, while the catalytic Zn^{2+} ion is illustrated as a gray sphere. The protein backbone is depicted as a light-blue cartoon, encompassing the wheat-colored protein surface that encircles the ligand. Amino acid side chains engaging in particular interactions with the ligand, as well as the ligands themselves, are visualized as sticks. Dashed yellow lines are utilized to represent polar interactions. Reproduced with permission from [100]. Copyright [2022] [Wiley-VCH].

3.2. Slow-binding class II HDAC inhibitors

Although slow-binding inhibitors have been developed mainly for targeting class I HDACs, recent studies have indicated that this approach can also be effective against other HDAC classes. For example, compound **22** (Figures 11 and 25) is a well-known HDAC inhibitor containing a trifluoromethyl ketone moiety as the ZBG.[13] Olsen *et al.* found that this compound

inhibited class IIa HDACs *via* a fast-on/fast-off mechanism, for which K_i values were 5.1 and 4.7 nM for HDAC4 and HDAC7, respectively. Compound **22**, on the other hand, exhibited slow-binding kinetics against class IIb enzymes. Specifically, compound **22** inhibited HDAC6, a class IIb HDAC isoform, *via* a slow-binding mechanism, for which K_i was 4.5 μM (Figure 25).
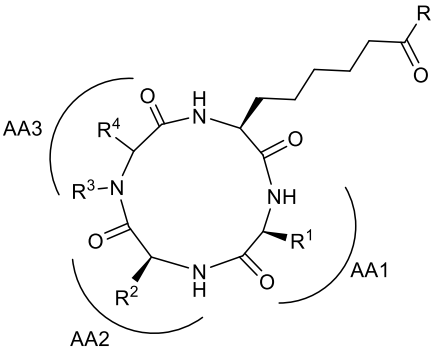

22

	HDAC4	HDAC6	HDAC7
K_i (nM)	5.1	4.5×10^3	4.7
k_1 (M^{-1} min^{-1})	-	2.6×10^3	-
k_{-1} (min^{-1})	-	1.2×10^{-2}	-

Figure 25. Chemical structure, K_i values, and kinetic parameters of class II HDAC inhibitor **22**.

In the previous section, we described a study by Olsen *et al.* on slow-binding inhibitors derived from natural products. The authors discovered several macrocycles that effectively inhibited class I HDACs by extending the drug–target residence time (Figure 9).[69] Moreover, the authors found that inhibitors **18** and **19** inhibited HDAC6 through a slow-binding mechanism, B (Scheme 1), as represented in Figure 26.

	R	AA1	AA2	AA3
18	NHOH	Phe	Phe	D-Pro
19	NHOH	Trp	Ile	D-Pip

|	**18**	**19**
k_{-2} (min^{-1})	0.0057	0.010
k_2 (min^{-1})	0.148	0.17
$K_{i,1}$ (nM)	34	23
K_i (nM)	~ 1.2	~ 3.6
t_R (min)	175	100

18, 19

Figure 26. Chemical structures and kinetic parameters of HDAC6 inhibitors **18** and **19**.

T-cell prolymphocytic leukemia (T-PLL) is an uncommon very aggressive cancer that affects hematological neoplasms. Reportedly, abnormal DNA damage and hypercytokine and growth factor responses trigger the neoplastic T-cell outgrowth, which is responsible for the migration of T-PLL cells.[101,102] This migratory T-cell phenotype could be controlled by regulating the activity of HDAC6.[101-103] Despite the development of several HDAC6 inhibitors, the inhibitor selectivity for other HDAC family members *in vitro* is only modest (approximately 5 or 6 times). Additionally, the inhibitor selectivity for HDAC6 *in vivo* is insufficient.[104-106] To overcome these limitations, Gunning *et al.* developed a highly potent and selective HDAC6 inhibitor that is particularly effective for treating T-PLL.[107] The authors comprehensively studied their previously reported inhibitor (**48**)[108] to develop a class of HDAC6-selective inhibitors based on a perfluorinated benzenesulfonamide moiety (Figure 27a). Although inhibitor **49** exhibited a very strong inhibitory potency against HDAC6 (for which IC_{50} was 0.9 nM), it was only moderately stable in glutathione (GSH). Therefore, the authors optimized the stability of inhibitor **49** to develop another HDAC6 inhibitor (**50**), which then exhibited a selectivity more than 39-fold higher for HDAC6 than for other HDACs and a higher cytotoxicity ($IC_{50} = 0.42$ μM) than another HDAC6 inhibitor, Nexturastat A ($IC_{50} = 1.68$ μM), in MV4-11 cancer cells.[109,110] In HeLa cells, inhibitor **50** induced the acetylation of α-tubulin, an HDAC 6 substrate, without affecting the acetylation of histone H3, which is a substrate for class I HDACs. Compared with citarinostat, a phase II clinical candidate, inhibitor **50** exhibited a higher selectivity for HDAC6 and an improved acetylation profile. Kinetic studies revealed that compared with inhibitors **48** and **49**, inhibitor **50** showed a considerably longer residence time *in vitro*, including 21- and 2.16-fold increases over **49** and **48**, respectively. This prolonged target interaction may have contributed to the inhibitor's selectivity, indicating that it functions as a slow-binding inhibitor for HDAC6. Gunning *et al.* continued their research for optimizing inhibitor **50** by developing a second-generation

inhibitor **51**, which retained the original potency (IC$_{50}$ = 8.9 nM for HDAC6) and exhibited a considerably improved selectivity (>200–550-fold) for HDAC6 over other isoforms.[111] Notably, compound **51** also showed therapeutic efficacy for treating metastatic Group 3 medulloblastoma (MB), which is the most common, aggressive, and malignant pediatric brain cancer. Intriguingly, inhibitor **51** exhibited a potentially enhanced (45-fold) selectivity for HDAC6, compared with citarinostat. Although the *in vitro* residence time of inhibitor **51** was only 8 min, the residence time in HeLa cells showed a longer target engagement of 97 min, which suggests that inhibitor **51** slowly dissociated from the target enzyme. In the *in silico* docking analysis of compound **50** (Figure 27b), a crucial interaction involving sandwich-type π–π interactions with Phe620 and Phe680 in the HDAC6 pocket was observed. This interaction contributed to a binding free energy of -8.30 kcal/mol, indicating strong binding affinity. Furthermore, despite lacking the F group, compound **50** still formed a hydrogen bond with the nearby Phe679 amide, suggesting its potential to interact favorably with the HDAC6 pocket and exhibit inhibitory activity. An additional π–π interaction between the fluorinated ring and surface residue His500 with a binding free energy of −7.966 kcal/mol (Figure 27c) was observed for inhibitor **51**. Further analysis of the X-ray crystal structures of inhibitors **50** and **51** (Figure 27d) showed that the isopropyl substitution in **51** generated an intramolecular π–π stacking interaction which could function as a steric barrier to prevent an attack from endogenous nucleophiles, such as GSH. Additionally, this is probably why the inhibitor **51** residence time was enhanced, which, in turn, improved the potency and selectivity for HDAC6. In MV4-11 cells, the minimum compound **51** dosage (0.1 μM) was sufficient to acetylate α-tubulin, and the histone H3 acetylation was limited at the highest concentration (5 μM). In contrast, at concentrations above 0.1 μM, the clinical candidate, citarinostat, showed off-target histone H3 acetylation effects. These findings suggested that for HDAC6, the selectivity profile of inhibitor **51** was considerably better than that of citarinostat because the dosage of inhibitor

51 required for the off-target acetylation was 50-fold higher than that of the citarinostat. Furthermore, HD-MB03 cells treated with inhibitor **51** showed a 44.3-fold improved therapeutic margin in primary MB cells compared to healthy neural stem cells. In addition, compound **51** showed a 45-fold increased potency compared to citarinostat.

(a)
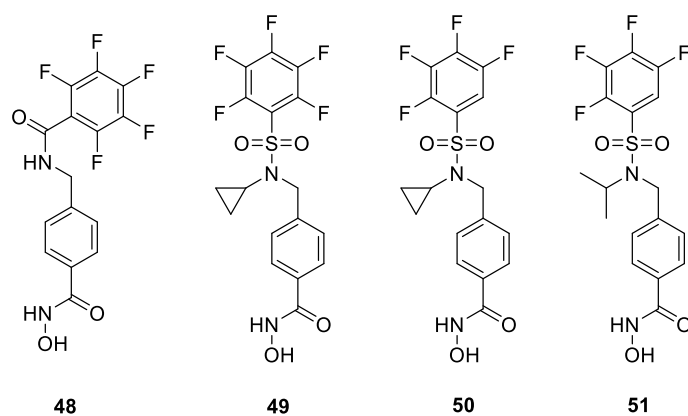
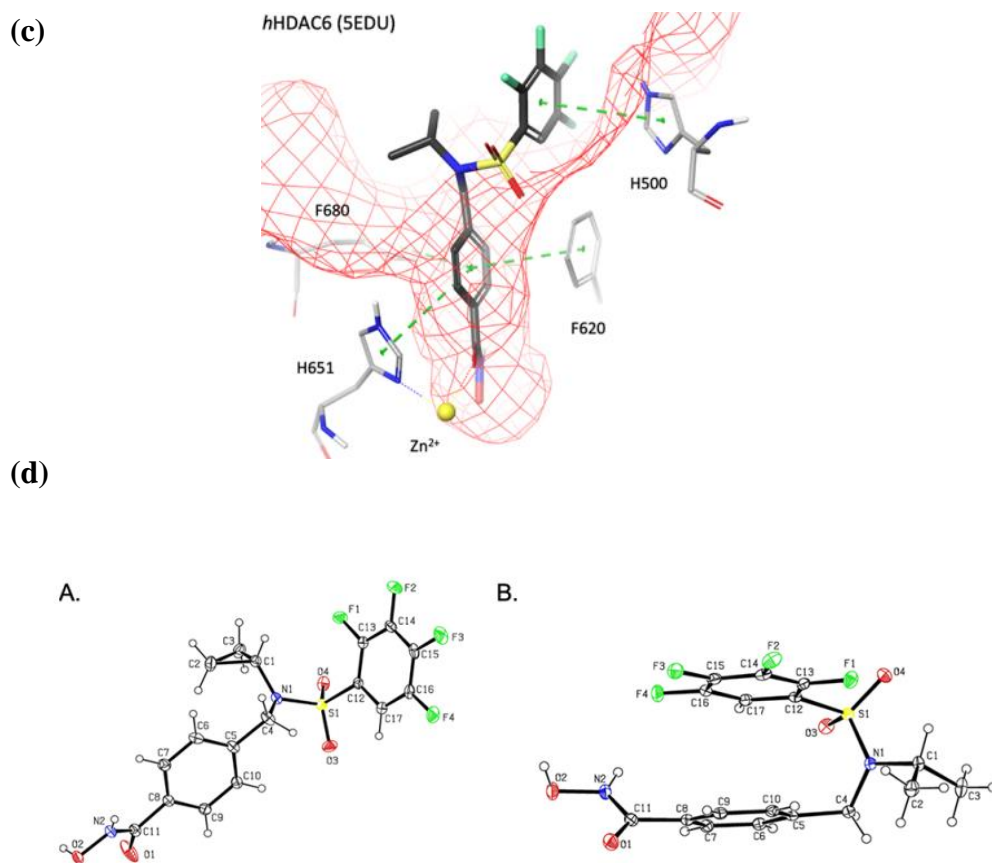|	in vitro				in vivo		
Compound	**48**	**49**	**50**	**51**	**50**	**51**	**Vorinostat**
k_{off} (s^{-1})	0.00156	0.015163	0.000718	0.00208	-	-	-
t_R (min)	10.716	1.0991	23.184	8.00	52	97	42

(b)

52

(c)

(d)
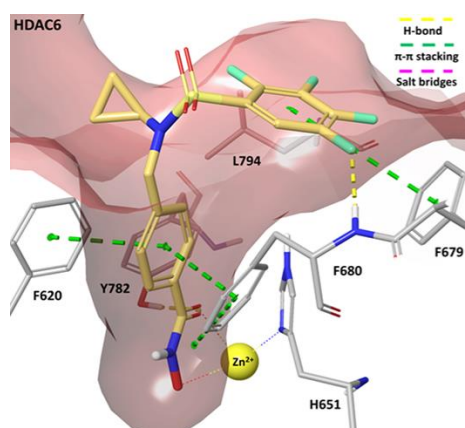
Figure 27. (a) Chemical structures and kinetic parameters of HDAC6 inhibitors **48**–**51**; (b) Binding interaction of **50** with human HDAC6 (PDB 5EDU), representing Zn^{2+} (yellow sphere), hydrogen bonds (yellow dashed line), π–π stacking (green dashed line), and salt bridges (purple dashed line) (N, blue; O, red; C, yellow; F, green). Reproduced with permission from [107]. Copyright [2021] [American Chemical Society]; (c)Binding interaction of **51** with human HDAC6 (PDB 5EDU), representing Zn^{2+} (yellow sphere), π–π stacking (green dashed line) (N, blue; O, red; C, black; F, green; S, yellow). Reproduced with permission from [111]. Copyright [2022] American Chemical Society; (d) X-ray crystal structure of inhibitor **50** (A) and **51** (B). Reproduced with permission from [111]. Copyright [2022] [American Chemical Society].

In a recent study led by Steinkuhler *et al.*, a new class of compounds (**52a-c**) was discovered as potent HDAC6 inhibitors.[112] Remarkably, these compounds displayed exceptional selectivity, exhibiting a preference of over 104-fold for HDAC6 in comparison to all other HDAC subtypes. Exploring the mechanism of HDAC6 inhibition by compound **52a** revealed a distinctive trait of slow-binding inhibition. As the duration of incubation increased, the degree of inhibition also progressively rose, signifying the presence of slow binding kinetics. Kinetic investigations confirmed that compound **52a** effectively inhibited HDAC6 through slow-binding mechanisms B (t_R = 3.6 to 5.1 h), as shown in Figure 28a. The analysis

of compound **52a** in interaction with zHDAC6-CD2 using docking simulations unveiled an intriguing binding mode (Figure 28b). The DFMO moiety formed a conventional dative bond with the Zn cation, facilitated by a nearby nitrogen atom at 2.4 Å. Despite its significant size, the DFMO group adeptly occupied the catalytic pocket, engaging specific residues and participating in π-π stacking with the His573-His574 dyad. Notably, an intriguing finding was the presence of residual empty space of approximately 60 Å3 near the DFMO group, Zn cation, His614, His573, and His574, which could accommodate a water molecule. This coexistence of a water molecule with a larger zinc-binding group (ZBG) like DFMO, compared to a hydroxamic acid, was unexpected. To elucidate differences in HDAC subtypes, this observation was compared with HDAC1 (a representative of class I enzymes). Discrepancies were attributed to the difluoromethyl-1,3,4-oxadiazole (DFMO) moiety's deeper penetration in class I enzymes, enabled by the availability of inner empty space. On the contrary, specific residues ($R_{569}P_{570}P_{571}$) in HDAC6 hindered such deep entry, creating an optimal orientation for nucleophilic attack. Additionally, a two-step hydrolytic conversion mechanism was proposed to explain selective inhibition. Compound **52a** was observed to undergo successive conversion into **52b** and then into **52c** when incubated with zHDAC6-CD2. The hydrolysis rate of **52a** was determined to be 6.04×10^{-3} min^{-1}, correlating with the measured k_{off} value, implying the presence of a hydrated derivative. The linear rate was attributed to the initial formation of the enzyme-inhibitor complex with a high dissociation constant. Furthermore, HDAC6 demonstrated the ability to convert **52b** into **52c**, indicating that both **52b** and **52c** serve as substrates for HDAC6.

(a)
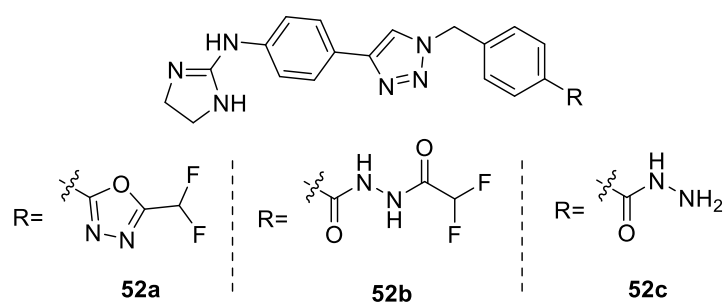
Compound	IC$_{50}$ (nM)	k_{on} (M^{-1}min^{-1})	k_{off} (min^{-1})^a	k_{off} (min^{-1})^b	K_i (nM)	t_R(h)^a	t_R(h)^b
52a	7.7	9.6 × 10^5	4.6 × 10^{-3}	3.3 × 10^{-3}	4.8	3.6	5.1

^{a}Calculated from k_{obs} plot. ^{b}Calculated from jump-dilution assay.

(b)
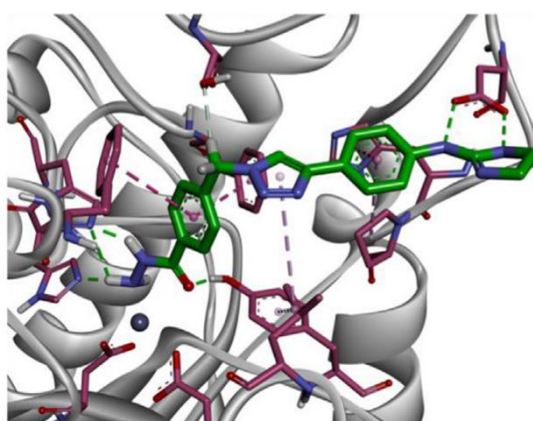
Figure 28. (a) Chemical structures and kinetic parameters of HDAC6 inhibitor **52**; (b) X-ray crystallographic analysis of the interaction between inhibitor **52a** and zHDAC6-CD2, in which the hydrazide **52c** securely bound within the catalytic core. Reproduced with permission from [112]. Copyright [2023] [American Society for Biochemistry and Molecular Biology].

3.3. Slow-binding class IV HDAC inhibitors

The prolonged residence time of slow-binding inhibitors requires a longer incubation time to inhibit the enzyme in *in vitro* enzyme assays. This can pose a challenge for unstable proteins, such as HDAC11, for which the activity is reduced by 40% when HDAC11 is incubated for 3 h at 37 °C.[113] However, some inhibitors function as chaperones, which correct misfolded conformations of the target protein.[114] Shen *et al.* assessed entinostat (**26**) (Figure 12) in an enzyme-based assay and found that **26** functioned as a slow-binding inhibitor for HDAC11, for

which IC_{50} was 0.9 µM, and required incubation for 3 h to equilibrate the binding.[113] At lower concentrations, entinostat **26** functioned as an agonist because HDAC11 was unstable. Owing to these findings, the researchers devised an assay protocol that utilized chaperone molecules to stabilize HDAC11 and discovered that the addition of vorinostat (0.2 µM) could stabilize the activity of HDAC11 during an assay for 3 h. Consequently, because 0.2 µM vorinostat inhibited 50% of the HDAC11 activity, the apparent IC_{50} value for **26** was adjusted to the true IC_{50} value (0.65 µM). Using this approach, the authors conducted a one-dose assay to screen several candidates. When chaperone molecules were not used, although false negative results were also obtained for inhibitors **53**, **54**, and **55** (Figure 29), inhibitors **53**, **54**, **55**, and **56** showed moderate inhibitory potencies for HDAC11 while maintaining their slow-binding profiles.
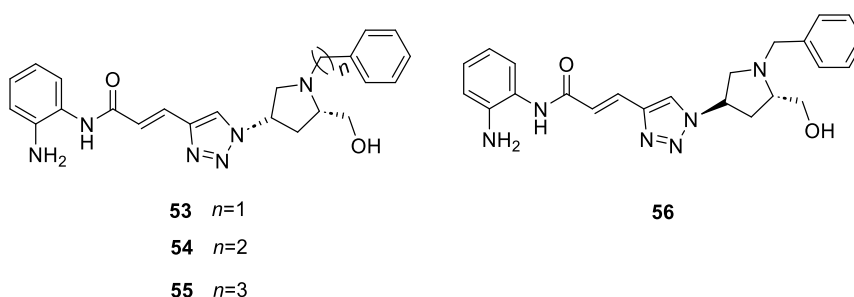

53 *n*=1
54 *n*=2
55 *n*=3

56

Figure 29. Chemical structures of HDAC11 inhibitors **53–56**.

Olsen *et al.* analyzed deacylation profiles for various zinc-dependent HDACs[115] and found that compared with other HDACs, HDAC11 showed an increased ability to remove long-chain ε-*N*-acyl lysine modifications (demyristoylation) where a hydroxamic-acid-containing macrocyclic peptide-based inhibitor **19** (Figures 9 and 30) effectively blocked the demyristoylation activity of HDAC11. In contrast, inhibitors, such as vorinostat, romidepsin, and epoxy ketone-based macrocyclic peptides, did not inhibit HDAC11. Further kinetic studies revealed that **19** acted through a slow-binding mechanism (B) (Scheme 1) to inhibit HDAC11, which prolonged the target engagement (Figure 30).
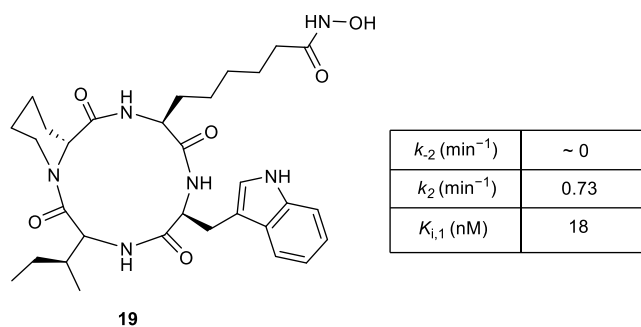
k_{-2} (min^{-1})	~ 0
k_2 (min^{-1})	0.73
$K_{i,1}$ (nM)	18

Figure 30. Chemical structure and kinetic parameters of HDAC11 inhibitor **19**.

4. Conclusion and perspectives

The development of drugs that can effectively inhibit disease-causing enzymes is an ongoing challenge for medicinal chemists. Enzymes are challenging targets because they have subclasses and isoforms, and designing subclass- or isoform-selective drugs is even more difficult. HDACs, a group of enzymes involved in the regulation of gene expression, have been implicated in various diseases, including cancer and neurodegenerative disorders. However, nonselective HDAC inhibitors can lead to unwanted side effects. Before Gottesfeld *et al.* reported the slow-binding inhibition by benzamide-based inhibitors in 2008, the validation of classical selective HDAC inhibitors was limited to thermodynamic parameters, such as IC$_{50}$ and K_d values. However, the work by Gottesfeld *et al.* highlighted the importance of the kinetic validation and determination of drug–target residence times for developing subclass- or isoform-selective HDAC drug candidates. Since then, the discovery of many HDAC inhibitors exhibiting prolonged target engagements has shown promise for developing subclass- or isoform-selective drugs that target HDACs. Although many slow-binding HDAC inhibitors have been assessed *in vitro* against class I HDACs, further research is required for establishing the efficacy of these inhibitors *in vivo*. Furthermore, although many studies have shown that drugs with longer residence times exhibit improved and prolonged *in vivo* activity in animal models (which can indicate the drugs' efficacy), precise molecular mechanisms underlying the

57

impact of t_R on drugs' *in vivo* pharmacological activities are still not fully understood. The rational design of slow-binding inhibitors requires a synergistic approach involving both experimental and computational methods.[10] This synergy aims to create compounds that establish enduring and stable complexes with the target enzyme, resulting in prolonged inhibition. This process would begin by conducting a thorough investigation of the enzyme's structure. This examination encompasses active site residues, as well as the identification of possible allosteric sites, which collectively establish the fundamental groundwork for the inhibitor design process. Critical insights from slow-binding inhibitors provide valuable insights into essential structural elements and interactions that contribute to this unique inhibition mechanism. Employing fragment-based drug design and optimizing linkers would facilitate the creation of larger molecules with enhanced binding kinetics. To validate the intended slow-binding characteristics, experimental verification becomes crucial. Techniques such as surface plasmon resonance (SPR) or stopped-flow spectroscopy play a pivotal role in confirming the desired slow-binding behaviour of the inhibitors. Notably, SPR-based off-rate screening offers an efficient approach to dynamically explore the chemical space from initial hits to lead compounds.[116,117] Nevertheless, specific subtype HDAC inhibitors such as HDAC9 are still lacking due to the limited understanding of HDAC9's precise function and its role in various cellular processes. The concept of slow-binding HDAC inhibitors is relatively new and is currently under investigation. As of now, there are no specific slow-binding HDAC inhibitors that are undergoing clinical trials. While there has been progress in understanding the mechanisms and potential of slow-binding inhibition, the only known slow-binding benzamide-based HDAC inhibitor "entinostat" has undergone comprehensive assessment in numerous phase I and II trials encompassing both solid and liquid tumors.[118] This perspective clearly summarizes the progress made in the development of slow-binding HDAC inhibitors and their action modes and potential clinical and therapeutic applications for treating cancers,

neurodegenerative disorders, and other diseases. Notably, the development of slow-binding inhibitors is not limited to HDACs, and further research can explore their applications for targeting enzyme classes other than HDACs.

AUTHOR INFORMATION

Corresponding Author

Takayoshi Suzuki − *SANKEN, Osaka University, Mihogaoka, Ibaraki-shi, Osaka 567-0047, Japan.*

*Email: tkyssuzuki@ sanken.osaka-u.ac.jp

Authors

Anirban Mukherjee − *SANKEN, Osaka University, Mihogaoka, Ibaraki-shi, Osaka 567-0047, Japan.*

Farzad Zamani − *SANKEN, Osaka University, Mihogaoka, Ibaraki-shi, Osaka 567-0047, Japan.*

Author Contributions

‡ A.M. and F.Z. contributed equally to this work.

Notes

Biographies

Anirban Mukherjee received his B.Sc. and M.Sc. from Visva Bharati University in 2015 and 2017 respectively. Following this, he worked as a junior research fellow at the National Institute of Pharmaceutical Education and Research (NIPER), Raebareli, focusing on developing new heterocyclic architectures as potential therapeutics using synthetic organic chemistry and DFT computational techniques (2018-2019). Subsequently, he served as a senior research fellow at CSIR-National Chemical Laboratory (NCL), Pune, where he worked on asymmetric synthesis (2020-2021). Anirban is currently a MEXT doctoral scholar at SANKEN, Osaka University, under the guidance of Professor Takayoshi Suzuki. His research primarily centers around utilizing novel medicinal chemistry tools for epigenetic drug discovery.

Farzad Zamani completed his PhD at the University of Wollongong (Australia) in 2019, where he worked on transition metal-catalysed reactions and heterocycle synthesis. He then joined the Professor Suzuki group at Osaka University as a JSPS postdoctoral fellow in 2020. During his time there, his research was primarily focused on the synthesis and investigation of small molecule epigenetic inhibitors in the field of drug discovery. He currently works at Pharmaxis (Australia), where he is involved in both the development and quality control processes of the company's commercial drugs.

Takayoshi Suzuki received his B.Sc. and M.Sc. from the University of Tokyo (1995 and 1997, respectively), after which he became a researcher at Japan Tobacco, Inc. (1997−2002). He subsequently joined Nagoya City University, Japan, as an assistant professor (2003− 2009) and later a lecturer (2009−2011). During that time, he received his Ph.D. from the Graduate School of Pharmaceutical Sciences, the University of Tokyo. He spent one year as a visiting investigator at the Scripps Research Institute, CA (Prof. M. G. Finn) (2007−2008). He was a

full-time professor at Kyoto Prefectural University of Medicine, Japan (2011 to 2019), and is currently a full-time professor at Osaka University (2019 to present). His research areas of interest are medicinal chemistry and bioorganic chemistry, including epigenetic drugs.

ABBREVIATIONS USED

BRET, bioluminescence resonance energy transfer; DFMO, difluoromethyl-1,3,4-oxadiazole; E, enzyme; E:I, enzyme-inhibitor; FRDA, friedreich ataxia; FXN, frataxin gene; FDA, U.S. food and drug administration; FTD, frontotemporal dementia; GFP, green fluorescent protein; GRN, progranulin gene; HDACs, histone deacetylase enzymes; HIV, human immunodeficiency virus; hERG, ether-a-go-go-related gene; IC_{50}, half maximal inhibitory concentration; I, inhibitor; [I], inhibitor concentration; IFNγ, interferon-gamma; iPSC, induced pluripotent stem cell; k_{on}, association rate constant; k_{off}, dissociation rate constant; KIKI, knock-in/knock-in; LPS, lipopolysaccharide; MB, medulloblastoma; NF-κB, nuclear factor κB; NcoR2, nuclear receptor co-repressor 2; PMBC, peripheral blood mononuclear cells; qRT-PCR, real-time quantitative reverse transcription PCR; [S], substrate concentration; SIRTs, Sirtuins; SAR, structure–activity relationship; SPR, surface plasmon resonance; $T_{1/2}$, dissociative half-life; t_R, residence time; T-PLL, T-cell prolymphocytic leukemia; ZBG, zinc binding group.

References

[1] Chaires, J. B. Calorimetry and thermodynamics in drug design. *Annu. Rev. Biophys.* **2008**, *37*, 135–151.

[2] Swinney, D. C. Biochemical mechanisms of drug action: What does it take for success? *Nature Rev. Drug Discov.* **2004**, *3*, 801–808.

[3] Copeland, R. A.; Pompliano, D. L.; Meek, T. D. Drug–target residence time and its implications for lead optimization. *Nature Rev. Drug Discov.* **2006**, *5*, 730–739.

[4] Copeland, R. A. The dynamics of drug–target interactions: Drug–target residence time and its impact on efficacy and safety. *Expert Opin. Drug Discov.* **2010**, *5*, 305–310.

[5] Copeland, R. A. The drug–target residence time model: A 10–year retrospective. *Nature Rev. Drug Discov.* **2016**, *15*, 87–95.

[6] Tummino, P. J.; Copeland, R. A. Residence time of receptor–ligand complexes and its effect on biological function. *Biochemistry* **2008**, *47*, 5481–5492.

[7] Dahl, G.; Akerud, T. Pharmacokinetics and the drug-target residence time concept. *Drug Discov. Today* **2013**, 18, 15–16.

[8] Lee, K. S. S.; Yang, J.; Niu, J.; Ng, C. J.; Wagner, K. M.; Dong, H.; Kodani, S. D.; Wan, D.; Morisseau, C.; Hammock, B. D. Drug-target residence time affects *in vivo* target occupancy through multiple pathways. *ACS Cent. Sci.* **2019**, *5*, 1614–1624.

[9] Callan, O. H.; So, O.-Y.; Swinney, D. C. The kinetic factors that determine the affinity and selectivity for slow binding inhibition of human prostaglandin H synthase 1 and 2 by indomethacin and flurbiprofen, *J. Biol. Chem.* **1996**, *271*, 3548– 3554.

[10] Mishima, H.; Itoh, Y.; Kurohara, T.; Suzuki, T.; Asada, N.; Kusakabe, K.; Okamoto, Y. Origin of the kinetic HDAC2-selectivity of an HDAC inhibitor. *J. Comput. Chem.* **2023**, *44*, 1604–1609.

[11] Hopkins, A. L.; Groom, C. R. The druggable genome. *Nat. Rev. Drug Discov.* **2002**, *1*, 727–730.

[12] Copeland, R. A. Conformational adaptation in drug-target interactions and residence time. *Future Med. Chem.* **2011**, *3*, 1491–1501.

[13] Madsen, A. S.; Olsen, C. A. A potent trifluoromethyl ketone histone deacetylase inhibitor exhibits class-dependent mechanism of action. *Med. Chem. Comm.* **2016**, *7*, 464–470.

[14] Goličnik, M.; Stojan, J. Slow–binding inhibition. *Biochem. Mol. Biol. Educ.* **2004**, *32*, 228–235.

[15] Morrison, J. F.; Walsh, C. T. The behaviour and significance of slow binding enzyme inhibitors. *Adv. Enzymol.* **1988**, *59*, 201–301.

[16] de Ruijter, A. J. M.; Gennip, A. H.; Caron, H. N.; Kemp, S.; van Kuilenburg, A. B. P. Histone deacetylases (HDACs): Characterization of the classical HDAC family. *Biochem. J.* **2003**, *370*, 737–749.

[17] Haberland, M.; Montgomery, R. L.; Olson, E. N. The many roles of histone deacetylases in development and physiology: Implications for disease and therapy. *Nat. Rev. Genet.* **2009**, *10*, 32–42.

[18] Roche, J.; Bertrand, P. Inside HDACs with more selective HDAC inhibitors. *Eur. J. Med. Chem.* **2016**, *121*, 451–483.

[19] Wang, D. -F.; Wiest, O.; Helquist, P.; Lan-Hargest, H. -Y.; Wiech, N. L. On the function of the 14 Å long internal cavity of histone deacetylase-like protein: Implications for the design of histone deacetylase inhibitors. *J. Med. Chem.* **2004**, *47*, 3409–3417.

[20] Bertrand, P. Inside HDAC with HDAC inhibitors. *Eur. J. Med. Chem.* **2010**, *45*, 2095–2116.

[21] Falkenberg, K. J.; Johnstone, R. W. Histone deacetylases and their inhibitors in cancer, neurological diseases and immune disorders. *Nature Rev. Drug Discov.* **2014**, *13*, 673–691.

[22] Glozak, M. A.; Seto, E. Histone deacetylases and cancer. *Oncogene* **2007**, *26*, 5420–5432.

[23] Shen, S.; Kozikowski, A. P. A patent review of histone deacetylase 6 inhibitors in neurodegenerative diseases (2014–2019). *Expert Opin. Ther. Pat.* **2020**, *30*, 121–136.

[24] Bondarev, A. D.; Attwood, M. M.; Jonsson, J.; Chubarev, V. N.; Tarasov, V. V.; Schiöth, H. B. Recent developments of HDAC inhibitors: Emerging indications and novel molecules. *Br. J. Clin. Pharmacol.* **2021**, *87*, 4577–4597.

[25] Finnin, M.; Donigian, J.; Cohen, J. A.; Richon, V. M.; Rifkind, R. A.; Marks, P. A.; Breslow, R.; Pavletich, N. P. Structures of a histone deacetylase homologue bound to the TSA and SAHA inhibitors. *Nature* **1999**, *401*, 188–193.

[26] Marks, P.; Xu, W. -S. Histone deacetylase inhibitors: Potential in cancer therapy. *J. Cell. Biochem.* **2009**, *107*, 600–608.

[27] Ho, C. S. T.; Chan, A. H. Y.; Ganesan, A. Thirty years of HDAC inhibitors: 2020 Insight and hindsight. *J. Med. Chem.* **2020**, *63*, 12460–12484.

[28] Leus, N. G. J.; Zwinderman, M. R. H.; Dekker, F. J. Histone deacetylase 3 (HDAC3) as emerging drug target in NF-κB-mediated inflammation. *Curr. Opin. Chem. Biol.* **2016**, *33*, 160–168.

[29] Li, G.; Tian, Y.; Zhu W. -G. The roles of histone deacetylases and their inhibitors in cancer therapy. *Front. Cell Dev. Biol.* **2020**, *8*, 576946.

[30] Maccallini, C.; Ammazzalorso, A.; De Filippis, B.; Fantacuzzi, M.; Giampietro, L.; Amoroso, R. HDAC inhibitors for the therapy of triple negative breast cancer, *Pharmaceuticals* **2022**, *15*, 667.

[31] Hammers, E. H.; Pili, R. Targeting tumor angiogenesis with histone deacetylase Inhibitors, *Cancer Lett.* **2009**, *280*, 145.

[32] Han, Y.; Nie, J.; Wang, D. W.; Ni, L. Mechanism of histone deacetylases in cardiac hypertrophy and its therapeutic inhibitors. *Front. Cardiovasc. Med.* **2022**, *9*, 931475.

[33] Shen, Z.; Bei, Y.; Lin, H.; Wei, T.; Dai, Y.; Hu, Y.; Zhang, C.; Dai, H. The role of class IIa histone deacetylases in regulating endothelial function. *Front. Physiol.* **2023**, *14*, 1091794.

[34] Guerriero, J. L.; Sotayo, A.; Ponichtera, H. E.; Castrillon, J. A.; Pourzia, A. L.; Schad, S.; Johnson, S. F.; Carrasco, R. D.; Lazo, S. Bronson, R. T.; Davis, S. P.; Lobera, M.; Nolan, M. A.; Letai, A. Class IIa HDAC inhibition reduces breast tumours and metastases through anti-tumour macrophages. *Nature* **2017**, *543*, 428–432.

[35] Yu, C. -W.; Chang, P. -T. Hsin, L. –W.; Chern, J. -W. Quinazolin-4-one derivatives as selective histone deacetylase-6 inhibitors for the treatment of Alzheimer's disease. *J. Med. Chem.* **2013**, *56*, 6775–6791.

[36] Adeshakin, A. O.; Adeshakin, F. O.; Yan, D.; Wan, X. Regulating histone deacetylase signaling pathways of myeloid-derived suppressor cells enhanced T cell-based immunotherapy, *Front. Immunol.* **2022**, *13*, Article 781660, 1–12.

[37] Son, S. I.; Cao, J.; Zhu, C. L.; Miller, S. P.; and Lin, H. Activity-guided design of HDAC11-specific inhibitors. *ACS Chem. Biol.* **2019**, *14*, 1393–1397.

[38] Sun, L.; de Evsikova, C. M.; Bian, K.; Achille, A.; Telles, E.; Pei, H.; Seto, E. Programming and regulation of metabolic homeostasis by HDAC11, *EBioMedicine* **2018**, *33*, 157–168.

[39] Cao, J.; Sun, L.; Aramsangtienchai, P., Spiegelman, N. A.; Zhang, X.; Huang, W.; Seto, E.; Lin, Hening. HDAC11 regulates type I interferon signaling through defatty-acylation of SHMT2. *Proc. Natl. Acad. Sci. USA* **2019**, 116, 5487–5492.

[40] Wilting, R. H.; Yanover, E.; Heideman, M. R.; Jacobs, H.; Horner, J.; van der Torre, J.; DePinho, R. A.; Dannenberg, J. H. Overlapping functions of HDAC1 and HDAC2 in cell cycle regulation and haematopoiesis. *EMBO J.* **2010**, *29*, 2586–2597.

[41] Hrzenjak, A.; Moinfar, F.; Kremser, M. -L.; Strohmeier, B.; Petru, E.; Zatloukal, K.; Denk, H. Histone deacetylase inhibitor vorinostat suppresses the growth of uterine sarcomas *in vitro* and *in vivo*. *Mol. Cancer* **2010**, *9*, Article number: 49.

[42] Thomas, S.; Miller, A.; Thurn, K. T.; Munster, P. Clinical applications of histone deacetylase inhibitors. *Handbook of Epigenetics*, Elsevier, **2011**, Pages 597–615.

[43] Bieliauskas, A. V.; Pflum, M. K. H.; Isoform-selective histone deacetylase inhibitors. *Chem. Soc. Rev.* **2008**, *37*, 1402–1413.

[44] Melesina, J.; Simoben, C. V.; Praetorius, L.; Bülbül, E. F.; Robaa, D.; Sippl, W. Strategies to design selective histone deacetylase inhibitors. *ChemMedChem* **2021**, *16*, 1336–1359.

[45] Meyners, C.; Baud, M. G. J.; Fuchter, M. J.; Meyer-Almes, F. -J. Kinetic method for the large-scale analysis of the binding mechanism of histone deacetylase inhibitors. *Anal. Biochem.* **2014**, *460*, 39–46.

[46] Wagner, F. F.; Zhang, Y. -L. Fass, D. M. Joseph, N. Gale, J. P. Weïwer, M.; McCarren, P.; Fisher, S. L.; Kaya, T.; Zhao, W. -N.; Reis, S. A.; Hennig, K. M.; Thomas, M.; Lemercier, B. C.; Lewis, M. C.; Guan, J. S.; Moyer, M. P.; Scolnick, E.; Haggarty, S. J.; Tsaia, L. -H.; Holson, E. B. Kinetically selective inhibitors of histone deacetylase 2 (HDAC2) as cognition enhancers. *Chem. Sci.* **2015**, *6*, 804–815.

[47] Wagner, F. F.; Weïwer, M.; Steinbacher, S.; Schomburg, A.; Reinemer, P.; Gale, J. P.; Campbell, A. J.; Fisher, S. L.; Zhao, W. -N.; Reis, S. A.; Hennig, K. M.; Thomas, M.; Müller, P.; Jefson, M. R.; Fass, D. M.; Haggarty, S. J.; Zhang, Y. -L.; Holson, E. B.; Kinetic and structural insights into the binding of histone deacetylase 1 and 2 (HDAC1, 2) inhibitors. *Bioorg. Med. Chem.* **2016**, *24*, 4008–4015.

[48] Wagner, F. F.; Lundh, M.; Kaya, T.; McCarren, P.; Zhang, Y. -L.; Chattopadhyay, S.; Gale, J. P.; Galbo, T.; Fisher, S. L.; Meier, B. C.; Vetere, A.; Richardson, S.; Morgan, N. G.; Christensen, D. P.; Gilbert, T. J.; Hooker, J. M.; Leroy, M.; Walpita, D.; Mandrup-Poulsen, T.; Wagner, B. K.; Holson, E. B. An isochemogenic set of inhibitors to define the therapeutic potential of histone deacetylases in β-cell protection. *ACS Chem. Biol.* **2016**, *11*, 363–374.

[49] Chou, C. J.; Herman, D.; Gottesfeld, J. M.; Pimelic diphenylamide 106 is a slow, tight-binding inhibitor of class I histone deacetylases. *J. Biol. Chem.* **2008**, *283*, 35402–35409.

[50] Wang, D. F.; Helquist, P.; Wiech, N. L.; Wiest, O. Toward selective histone deacetylase inhibitor design: Homology modeling, docking studies, and molecular dynamics simulations of human class I histone deacetylases. *J. Med. Chem.* **2005**, *48*, 6936–6947.

[51] Herman, D.; Jenssen, K.; Burnett, R.; Soragni, E.; Perlman, S. L.; Gottesfeld, J. M. Histone deacetylase inhibitors reverse gene silencing in Friedreich's ataxia. *Nat. Chem. Biol.* **2006**, *2*, 551–558.

[52] Gottesfeld, J. M. Small molecules affecting transcription in Friedreich ataxia. *Pharmacol. Ther.* **2007**, *116*, 236–248.

[53] Campuzano, V.; Montermini, L.; Molto, M. D.; Pianese, L.; Cossee, M.; Cavalcanti, F.; Monros, E.; Rodius, F.; Duclos, F.; Monticelli, A.; Zara, F.; Cañizares, J.; Koutnikova, H.; Bidichandani, S. I.; Gellera, C.; Brice, A.; Trouillas, P.; De Michele, G.; Filla, A.; De Frutos, R.; Palau, F.; Patel, P. I.; Di Donato, S.; Mandel, J. L.; Cocozza, S.; Koenig, M.; Pandolfo, M. Friedreich's ataxia: Autosomal recessive disease caused by an intronic GAA triplet repeat expansion. *Science* **1996**, *271*, 1423–1427.

[54] Soragni, E.; Miao, W.; Iudicello, M.; Jacoby, D.; Demercanti, S.; Clerico, M.; Longo, F.; Piga, A.; Ku, S.; Campau, E.; Du, J.; Penalver, P.; Rai, M.; Madara, J. C.; Nazor, K.; O'Connor, M.; Maximov, A.; Loring, J. F.; Pandolfo, M.; Durelli, L.; Gottesfeld, J. M.; Rusche, J. R. Epigenetic therapy for Friedreich's ataxia. *Ann. Neurol.* **2014**, *76*, 489–508.

[55] Rai, M.; Soragni, E.; Chou, C. J.; Barnes, G.; Jones, S.; Rusche, J. R.; Gottesfeld, J. M.; Pandolfo, M. Two new pimelic diphenylamide HDAC inhibitors induce sustained Frataxin upregulation in cells from Friedreich's ataxia patients and in a mouse model. *PLoS ONE* **2010**, *5*, e8825.

[56] Soragni, E.; Chou, C. J.; Rusche, J. R.; Gottesfeld, J. M.; Mechanism of action of 2-aminobenzamide HDAC inhibitors in reversing gene silencing in Friedreich's ataxia. *Front. Neurol.* **2015**, *6*, article 44, 1–11.

[57] Gryder, B. E.; Sodji, Q. H.; Oyelere, A. K. Targeted cancer therapy: Giving histone deacetylase inhibitors all they need to succeed. *Future Med. Chem.* **2012**, *4*, 505–524.

[58] Methot, J. L.; Hoffman, D. M.; Witter, D. J.; Stanton, M. G.; Harrington, P.; Hamblett, C.; Siliphaivanh, P.; Wilson, K.; Hubbs, J.; Heidebrecht, R.; Kral, A. M.; Ozerova, N.; Fleming, J. C.; Wang, H.; Szewczak, A. A.; Middleton, R. E.; Hughes, B.; Cruz, J. C.; Haines, B. B.; Chenard, M.; Kenific, C. M.; Harsch, A.; Secrist, J. P.; Miller, T. A. Delayed and prolonged histone hyperacetylation with a selective HDAC1/HDAC2 inhibitor. *ACS Med. Chem. Lett.* **2014**, *5*, 340–345.

[59] Kral, A. M.; Ozerova, N.; Close, J.; Jung, J.; Chenard, M.; Fleming, J.; Haines, B. B.; Harrington, P.; Maclean, J.; Miller, T. A.; Secrist, P.; Wang, H.; Heidebrecht Jr, R. W. Divergent kinetics differentiate the mechanism of action of two HDAC inhibitors, *Biochemistry* **2014**, *53*, 725–734.

[60] Molina, D. M.; Jafari, R.; Ignatushchenko, M.; Seki, T.; Larsson, E. A.; Dan, C.; Sreekumar, L.; Cao, Y.; Nordlund, P. Monitoring drug target engagement in cells and tissues using the cellular thermal shift assay. *Science* **2013**, *341*, 84–87.

[61] Moreau, M. J.; Morin, I.; Schaeffer, P. M. Quantitative determination of protein stability and ligand binding using a green fluorescent protein reporter system. *Mol. Biosyst.* **2010**, *6*, 1285–1292.

[62] Savitski, M. M.; Reinhard, F. B. M.; Franken, H.; Werner, T.; Savitski, M. F.; Eberhard, D.; Molina, D. M.; Jafari, R.; Dovega, R. B.; Klaeger, S.; Kuster, B.; Nordlund, P.; Bantscheff, M.; Drewes, G. Tracking cancer drugs in living cells by thermal profiling of the proteome. *Science* **2014**, *346*, 1255784.

[63] Machleidt, T.; Woodroofe, C. C.; Schwinn, M. K.; Méndez, J.; Robers, M. B.; Zimmerman, K.; Otto, P.; Daniels, D. L.; Kirkland, T. A.; Wood, K. V. NanoBRET-A novel BRET platform for the analysis of protein-protein interactions. *ACS Chem. Biol.* **2015**, *10*, 1797–1804.

[64] Robers, M. B.; Dart, M. L.; Woodroofe, C. C.; Zimprich, C. A.; Kirkland, T. A.; Machleidt, T.; Kupcho, K. R.; Levin, S.; Hartnett, J. R.; Zimmerman, K.; Niles, A. L.; Ohana, R. F.;

Daniels, D. L.; Slater, M.; Wood, M. G.; Cong, M.; Cheng, Y. -Q.; Wood, K. V. Target engagement and drug residence time can be observed in living cells with BRET. *Nat. Comm.* **2015**, *3*, 10091.

[65] Maolanon, A. R.; Kristensen, H. M.; Leman, L. J.; Ghadiri, M. R.; Olsen, C. A. Natural and synthetic macrocyclic inhibitors of the histone deacetylase enzymes. *ChemBioChem* **2017**, *18*, 5–49.

[66] Ito, T.; Umehara, T.; Sasaki, K.; Nakamura, Y.; Nishino, N.; Terada, T.; Shirouzu, M.; Padmanabhan, B.; Yokoyama, S.; Ito, A.; Yoshida, M. Real-time imaging of histone H4K12-specific acetylation determines the modes of action of histone deacetylase and bromodomain inhibitors. *Chem. Biol.* **2011**, *18*, 495–507.

[67] Montero, A.; Beierle, J. M.; Olsen, C. A.; Ghadiri, M. R. Design, synthesis, biological evaluation, and structural characterization of potent histone deacetylase inhibitors based on cyclic α/β-tetrapeptide architectures. *J. Am. Chem. Soc.* **2009**, *131*, 3033–3041.

[68] Vickers, C. J.; Olsen, C. A.; Leman, L. J.; Ghadiri, M. R. Discovery of HDAC inhibitors that lack an active site Zn^{2+}-binding functional group. *ACS Med. Chem. Lett.* **2012**, *3*, 505–508.

[69] Kitir, B.; Maolanon, A. R.; Ohm, R. G.; Colaço, A. R.; Fristrup, P.; Madsen, A. S.; Olsen, C. A. Chemical editing of macrocyclic natural products and kinetic profiling reveal slow, tight-binding histone deacetylase inhibitors with picomolar affinities. *Biochemistry* **2017**, *56*, 5134–5146.

[70] Hobara, T.; Uchida, S.; Otsuki, K.; Matsubara, T.; Funato, H.; Matsuo, K.; Suetsugi, M.; Watanabe, Y. Altered gene expression of histone deacetylases in mood disorder patients. *J. Psychiatr. Res.* **2010**, *44*, 263–270.

[71] Tsankova, N. M.; Kumar, A.; Nestler, E. J. Histone modifications at gene promoter regions in rat hippocampus after acute and chronic electroconvulsive seizures. *J. Neurosci.* **2004**, *24*, 5603–5610.

[72] Schroeder, F. A.; Lin, C. L.; Crusio, W. E.; Akbarian, S. Antidepressant-like effects of the histone deacetylase inhibitor, sodium butyrate, in the mouse. *Biol Psychiatry* **2007**, *62*, 55–64.

[73] Schroeder, F. A.; Lewis, M. C.; Fass, D. M.; Wagner, F. F.; Zhang, Y. -L.; Hennig, K. M.; Gale, J.; Zhao, W. -N.; Reis, S.; Barker, D. D.; Berry-Scott, E.; Kim, S. W.; Clore, E. L.; Hooker, J. M.; Holson, E. B.; Haggarty, S. J.; Petryshen, T. L. A selective HDAC1/2 inhibitor modulates chromatin and gene expression in brain and alters mouse behavior in two mood-related tests. *Plos One* **2013**, *8*, e71323.

[74] Covington, H. E.; Antidepressant actions of histone deacetylase inhibitors. *J. Neurosci.* **2009**, *29*, 11451–11460.

[75] Allen, K. N.; Abeles, R. H. Inhibition kinetics of acetylcholinesterase with fluoromethyl ketones. *Biochemistry* **1989**, *28*, 8466–8473.

[76] Nielsen, T. K.; Hildmann, C.; Riester, D.; Wegener, D.; Schwienhorst, A.; Ficner, R. Complex structure of a bacterial class 2 histone deacetylase homologue with a trifluoromethylketone inhibitor. *Acta Crystallogr., Sect. F: Struct. Biol. Cryst. Comm.* **2007**, *63*, 270–273.

[77] Brady, K.; Abeles, R. H. Inhibition of chymotrypsin by peptidyl trifluoromethyl ketones: Determinants of slow-binding kinetics. *Biochemistry* **1990**, *29*, 7608–7617.

[78] Gelb, M. H.; Svaren, J. P.; Abeles, R. H. Fluoro ketone inhibitors of hydrolytic enzymes. *Biochemistry* **1985**, *24*, 1813–1817.

[79] Ourailidou, M. E.; Leus, N. G. J.; Krist, K.; Lenoci, A.; Mai, A.; Dekker, F. J. Chemical epigenetics to assess the role of HDAC1–3 inhibition in macrophage pro-inflammatory gene expression. *Med. Chem. Comm.* **2016**, *7*, 2184–2190.

[80] Shakespear, M. R.; Halili, M. A.; Irvine, K. M.; Fairlie, D. P.; Sweet, M. J.; Histone deacetylases as regulators of inflammation and immunity. *Trends Immunol.* **2011**, *32*, 335–343.

[81] McKinsey, T. A. Therapeutic potential for HDAC inhibitors in the heart. *Annu. Rev. Pharmacol. Toxicol.* **2012**, *52*, 303–319.

[82] Lauffer, B. E. L.; Mintzer, R.; Fong, R.; Mukund, S.; Tam, C.; Zilberleyb, I.; Flicke, B.; Ritscher, A.; Fedorowicz, G.; Vallero, R.; Ortwine, D. F.; Gunzner, J.; Modrusan, Z.; Neumann, L.; Koth, C. M.; Lupardus, P. J.; Kaminker, J. S.; Heise, C. E.; Steiner, P. Histone deacetylase (HDAC) inhibitor kinetic rate constants correlate with cellular histone acetylation but not transcription and cell viability. *J. Biol. Chem.* **2013**, *288*, 26926–2643.

[83] van Swieten, J. C.; Heutink, P. Mutations in progranulin (GRN) within the spectrum of clinical and pathological phenotypes of frontotemporal dementia. *Lancet Neurol.* **2008**, *7*, P965–974.

[84] Cenik, B.; Sephton, C. F.; Dewey, C. M.; Xian, X.; Wei, S.; Yu, K.; Niu, W.; Coppola, G.; Coughlin, S. E.; Lee, S. E.; Dries, D. R.; Almeida, S.; Geschwind, D. H.; Gao, F. -B.; Miller, B. L.; Farese Jr, R. V.; Posner, B. A.; Yu, G.; Herz, J. Suberoylanilide hydroxamic acid (vorinostat) up-regulates progranulin transcription. *J. Biol. Chem.* **2011**, *286*, P16101–16108.

[85] She, A.; Kurtser, I.; Reis, S. A.; Hennig, K.; Lai, J.; Lang, A.; Zhao, W. -N.; Mazitschek, R.; Dickerson, B. C.; Herz, J.; Haggarty, S. J. Selectivity and kinetic requirements of HDAC inhibitors as progranulin enhancers for treating frontotemporal dementia. *Cell Chem. Biol.* **2017**, *24*, P892–906.

[86] Moreno-Yruela, C.; Fass, D. M.; Cheng, C.; Herz, J.; Olsen, C. A.; Haggarty, S. J. Kinetic tuning of HDAC inhibitors affords potent inducers of progranulin expression. *ACS Chem. Neurosci.* **2019**, *10*, 3769–3777.

[87] Moreno-Yruela, C.; Olsen, C. A. Determination of slow-binding HDAC inhibitor potency and subclass selectivity. *ACS Med. Chem. Lett.* **2022**, *13*, 779–785.

[88] Huber, K.; Doyon, G.; Plaks, J.; Fyne, E.; Mellors, J. W.; Sluis-Cremer, N. Inhibitors of histone deacetylases: Correlation between isoform specificity and reactivation of HIV type 1 (HIV-1) from latently infected cells. *J. Biol. Chem.* **2011**, *286*, 22211–22218.

[89] Liu, J.; Yu, Y.; Kelly, J.; Sha, D.; Alhassan, A. -B.; Yu, W.; Maletic, M. M.; Duffy, J. L.; Klein, D. J.; Holloway, M. K.; Carroll, S.; Howell, B. J.; Barnard, R. J. O.; Wolkenberg, S.; Kozlowski, J. A. Discovery of highly selective and potent HDAC3 inhibitors based on a 2 substituted benzamide zinc binding group. *ACS Med. Chem. Lett.* **2020**, *11*, 2476–2483.

[90] Zhou, J.; Li, M.; Chen, N.; Wang, S.; Luo, H. -B.; Zhang, Y.; Wu, R. Computational design of a time-dependent histone deacetylase 2 selective inhibitor. *ACS Chem. Biol.* **2015**, *10*, 687–692.

[91] Chen, C.; Sethy, B.; Liou, J. -P. Recent update of HDAC inhibitors in lymphoma. *Front. Cell Dev. Biol.* **2020**, *8*, Article 586391.

[92] McClure, J. J.; Zhang, C.; Inks, E. S.; Peterson, Y. K.; Li, J.; Chou, C. J. Class I HDAC inhibitors display different antitumor mechanism in leukemia and prostatic cancer cells depending on their p53 status. *J. Med. Chem.* **2018**, *61*, 2589−2603.

[93] Li, X.; Zhang, Y.; Jiang, Y.; Wu, J.; Inks, E. S.; Chou, C. J.; Gao, S.; Hou, J.; Ding, Q.; Li, J. Selective HDAC inhibitors with potent oral activity against leukemia and colorectal cancer: Design, structure-activity relationship and anti-tumor activity study. *Eur. J. Med. Chem.* **2017**, *134*, 185–206.

[94] Li, X.; Jiang, Y.; Peterson, Y. K.; Xu, T.; Himes, R. A.; Luo, X.; Yin, G.; Inks, E. S.; Dolloff, N.; Halene, S.; Chan, S. S. L.; Chou, C. J. Design of hydrazide-bearing HDACIs based on panobinostat and their p53 and FLT3-ITD dependency in anti-leukemia activity. *J. Med. Chem.* **2020**, *63*, 5501–5525.

[95] Mao, P. -T.; He, W. -B.; Mai, X.; Feng, L. -H.; Li, N.; Liao, Y. -J.; Zhu, C. -S.; Li, J.; Chen, T.; Liu, S. -H.; Zhang, Q. -M.; He, L. Synthesis and biological evaluation of

aminobenzamides containing purine moiety as class I histone deacetylases inhibitors. *Bioorg. Med. Chem.* **2022**, *56*, 116599.

[96] Suzuki, T. Explorative study on isoform-selective histone deacetylase inhibitors. *Chem. Pharm. Bull.* **2009**, *57*, 897–906.

[97] Yue, K.; Qin, M.; Huang, C.; Chou, C. J.; Jiang, Y.; Li, X.; Comparison of three zinc binding groups for HDAC inhibitors – A potency, selectivity and enzymatic kinetics study. *Bioorg. Med. Chem. Lett.* **2022**, *70*, 128797.

[98] Suzuki, T.; Itoh, Y.; Tojo, T.; Uchida, S. Histone deacetylase inhibitor. *Patent Appl.* **2019**, WO 2019235501.

[99] Wang, Y.; Stowe, R. L.; Pinello, C. E.; Tian, G.; Madoux, F.; Li, D.; Zhao, L. Y.; Li, J.-L.; Wang, Y.; Wang, Y.; Ma, H.; Hodder, P.; Roush, W. R.; Liao, D. Identification of histone deacetylase inhibitors with benzoylhydrazide scaffold that selectively inhibit class I histone deacetylases. *Chem. Biol.* **2015**, *22*, 273−284.

[100] Schäker-Hübner, L.; Haschemi, R.; Büch, T.; Kraft, F. B.; Brumme, B.; Schöler, A.; Jenke, R.; Meiler, J.; Aigner, A.; Bendas, G.; Hansen, F. K. Balancing histone deacetylase (HDAC) inhibition and drug-likeness: Biologicaland physicochemical evaluation of class I selective HDAC inhibitors. *ChemMedChem* **2022**, *17*, e202100755.

[101] Herling, M.; Khoury, J. D.; Washington, L. B. T.; Duvic, M.; Keating, M. J.; Jones, D. A Systematic approach to diagnosis of mature T-cell leukemias reveals heterogeneity among WHO categories. *Blood* **2004**, *104*, 328–335.

[102] Wahnschaffe, L.; Braun, T.; Timonen, S.; Giri, A. K.; Schrader, A.; Wagle, P.; Almusa, H.; Johansson, P.; Bellanger, D.; López, C.; Haferlach, C.; Stern, M.; Durig, J.; Siebrt, R.; Mustjoki, S.; Aittokallio, T.; Herling, M. Jak/Stat-activating genomic alterations are a hallmark of T-PLL. *Cancers* **2019**, *11*, 1833.

[103] He, L.; Tang, J.; Andersson, E. I.; Timonen, S.; Koschmieder, S.; Wennerberg, K.; Mustjoki, S.; Aittokallio, T. Patient-customized drug combination prediction and testing for T-cell prolymphocytic leukemia patients. *Cancer Res.* **2018**, *78*, 2407–2418.

[104] Haggarty, S. J.; Koeller, K. M.; Wong, J. C.; Grozinger, C. M.; Schreiber, S. L. Domain-selective small-molecule inhibitor of histone deacetylase 6 (HDAC6)-mediated tubulin deacetylation. *PNAS* **2003**, *100*, 4389–4394.

[105] Huang, P.; Almeciga-Pinto, I.; Jarpe, M.; van Duzer, J. H.; Mazitschek, R.; Yang, M.; Jones, S. S.; Quayle, S. N. Selective HDAC inhibition by ACY-241 enhances the activity of paclitaxel in solid tumor models. *Oncotarget* **2017**, *8*, 2694–2707.

[106] Santo, L.; Hideshima, T.; Kung, A. L.; Tseng, J. -C.; Tamang, D.; Yang, M.; Jarpe, M.; van Duzer, J. H.; Mazitschek, R.; Ogier, W. C.; Cirstea, D.; Rodig, S.; Eda, H.; Scullen, T.; Canavese, M.; Bradner, J.; Anderson, K. C.; Jones, S. S.; Raje, N. Preclinical activity, pharmacodynamic, and pharmacokinetic properties of a selective HDAC6 inhibitor, ACY-1215, in combination with bortezomib in multiple myeloma. *Blood* **2012**, *119*, 2579–2589.

[107] Toutah, K.; Nawar, N.; Timonen, S.; Sorger, H.; Raouf, Y. S.; Bukhari, S.; von Jan, J.; Ianevski, A.; Gawel, J. M.; Olaoye, O. O.; Geletu, M.; Abdeldayem, A.; Israelian, J.; Radu, T. B.; Sedighi, A.; Bhatti, M. N.; Hassan, M. M.; Manaswiyoungkul, P.; Shouksmith, A. E.; Neubauer, H. A.; de Araujo, E. D.; Aittokallio, T.; Krämer, O. H.; Moriggl, R.; Mustjoki, S.; Herling, M.; Gunning, P. T. Development of HDAC inhibitors exhibiting therapeutic potential in T-cell prolymphocytic leukemia. *J. Med. Chem.* **2021**, *64*, 8486–8509.

[108] Gawel, J. M.; Shouksmith, A. E.; Raouf, Y. S.; Nawar, N.; Toutah, K.; Bukhari, S.; Manaswiyoungkul, P.; Olaoye, O. O.; Israelian, J.; Radu, T. B.; Cabral, A. D.; Sina, D.; Sedighi, A.; de Araujo, E. D.; Gunning, P. T. PTG-0861: A novel HDAC6-selective inhibitor as a therapeutic strategy in acute myeloid leukaemia. *Eur. J. Med. Chem.* **2020**, *201*, 112411.

[109] Bergman, J. A.; Woan, K.; Perez-Villarroel, P.; Villagra, A.; Sotomayor, E. M.; Kozikowski, A. P. Selective histone deacetylase 6 inhibitors bearing substituted urea linkers inhibit melanoma cell growth. *J. Med. Chem.* **2012**, *55*, 9891−9899.

[110] Woan, K. V.; Lienlaf, M.; Perez-Villaroel, P.; Lee, C.; Cheng, F.; Knox, T.; Woods, D. M.; Barrios, K.; Powers, J.; Sahakian, E.; Wang, H. W.; Canales, J.; Marante, D.; Smalley, K. S. M.; Bergman, J.; Seto, E.; Kozikowski, A.; Pinilla-Ibarz, J.; Sarnaik, A.; Celis, E.; Weber, J.; Sotomayor, E. M.; Villagra, A. Targeting histone deacetylase 6 mediates a dual anti-melanoma effect: Enhanced antitumor immunity and impaired cell proliferation. *Mol. Oncol.* **2015**, *9*, 1447−1457.

[111] Nawar, N.; Bukhari, S.; Adile, A. A.; Suk, Y.; Manaswiyoungkul, P.; Toutah, K.; Olaoye, O. O.; Raouf, Y. S.; Sedighi, A.; Garcha, H. K.; Hassan, M. M.; Gwynne, W.; Israelian, J.; Radu, T. B.; Geletu, M.; Abdeldayem, A.; Gawel, J. M.; Cabral, A. D.; Venugopal, C.; de Araujo, E. D.; Singh, S. K.; Gunning, P. T. Discovery of HDAC6-selective inhibitor NN-390 with in vitro efficacy in group 3 medulloblastoma. *J. Med. Chem.* **2022**, *65*, 3193−3217.

[112] Cellupica, E.; Caprini, G.; Cordella, P.; Cukier, C.; Fossati, G.; Marchini, M.; Rocchio, I.; Sandrone, G.; Vanoni, M. A.; Vergani, B.; Zrubek, K.; Stevenazzi, A.; Steinkuhler, C. Difluoromethyl-1,3,4-oxadiazoles are slow-binding substrate analog inhibitors of histone deacetylase6 with unprecedented isotype selectivity. *J. Biol. Chem.* **2023**, *299*, 102800.

[113] Tian, Y.; Lv, W.; Li, X.; Wang, C.; Wang, D.; Wang, P. G.; Jin, J.; Shen, J. Stabilizing HDAC11 with SAHA to assay slow-binding benzamide inhibitors. *Bioorg. Med. Chem. Lett.* **2017**, *27*, 2943–2945.

[114] Rajan, R. S.; Tsumoto, K.; Tokunaga, M.; Tokunaga, H.; Kita, Y.; Arakawa, T. Chemical and pharmacological chaperones: Application for recombinant protein production and protein folding diseases. *Curr. Med. Chem.* **2011**, *18*, 1–15.

[115] Moreno-Yruela, C.; Galleano, I.; Madsen, A. S.; Olsen, C. A. Histone deacetylase 11 is an ε-N-myristoyllysine hydrolase. *Cell Chem. Biol.* **2018**, *25*, 849–856.

[116] Liu, L. Efficient hit and lead compound evaluation strategy based on off-rate screening by surface plasmon resonance. *J. Med. Chem.* **2014**, *57*, 2843–2844.

[117] Murray, J. B.; Roughley, S. D.; Matassova, N.; Brough, P. A. Off-rate screening (ORS) by surface plasmon resonance. An efficient method to kinetically sample hit to lead Chemical space from unpurified reaction products. *J. Med. Chem.* **2014**, *57*, 2845-2850.

[118] Connolly, R. M.; Rudek, M. A.; Piekarz, R. Entinostat: a promising treatment option for patients with advanced breast cancer. *Future Oncol.* **2017**, *13*, 1137.

TOC graphic